Guilherme Ornelas Pimentel Meneses

Licenciatura em Engenharia Biomédica

Electron driven reactions in sulphur containing biological prototypes

Dissertação para obtenção do Grau de
Mestre em Engenharia Biomédica

Orientador: Doutor Filipe Ribeiro Ferreira da Silva,
Investigador Pos-Doc, Universidade Nova de Lisboa

Júri:

Presidente:	Prof. Doutora Carla Maria Quintão Pereira
Arguente:	Prof. Doutora Maria José Diogo da Silva Calhorda
Vogal:	Prof. Doutor Filipe Ferreira da Silva

FACULDADE DE
CIÊNCIAS E TECNOLOGIA
UNIVERSIDADE NOVA DE LISBOA

Maio, 2015

Electron driven reactions in sulphur containing biological prototypes

Acknowledgements

I would like to express my special appreciation and thanks to my advisor Dr. Filipe Ferreira da Silva, for his constant support, encouragement and for the opportunity he has given me to visit and work with an international group. You have been a tremendous mentor for me.

Prof. Dr. Janina Kopyra, for her supervision, discussion and assistance while and after working at the Siedlce University.

Prof. Dr. Paulo Limão-Vieira for the immense knowledge and guidance throughout these years. Special thanks to Diogo Almeida for all the help, availability and laughs. Tiago Cunha for the fruitful discussions, hard work and friendship through the several stages of this thesis.

I thank all of the remaining members of the research group, particularly Dr. Susana Sério, Juscelino Ferreira and Emanuele Lange.

NANO-IBCT for providing me with financial support for the STSM. To the Department of Physics of the New University of Lisbon, CEFITEC, and Siedlce University for providing me the necessary working conditions.

My cousin Diogo, Paulo and his colleagues for their help and availability.

My closest colleagues and friends from UNL, not only for the much-valued friendship but also for all the great moments shared over the years.

To my dedicated parents, for the unconditional support.

Rita, for the relentless love and encouragement, and for believing in me. I am sure I could not have done it without it.

Abstract

The interaction of ionising radiation with living tissues may direct or indirectly generate several secondary species with relevant genotoxic potential.

Due to recent findings that electrons with energies below the ionisation threshold can effectively damage DNA, radiation-induced damage to biological systems has increasingly come under scrutiny. The exact physico-chemical processes that occur in the first stages of electron induced damage remain to be explained. However, it is also known that free electrons have a short lifetime in the physiological medium. Hence, electron transfer processes studies represent an alternative approach through which the role of "bound" electrons as a source of damage to biological tissues can be further explored.

The thesis work consists of studying dissociative electron attachment (DEA) and electron transfer to taurine and thiaproline. DEA measurements were executed in Siedlce University with Prof. Janina Kopyra under COST action MP1002 (Nanoscale insights in ion beam cancer therapy). The electron transfer experiments were conducted in a crossed atom(potassium)-molecule beam arrangement.

In these studies the anionic fragmentation patterns were obtained. The results of both mechanisms are shown to be significantly different, unveiling that the damaging potential of secondary electrons can be underestimated. In addition, sulphur atoms appear to strongly influence the dissociation process, demonstrating that certain reactions can be controlled by substitution of sulphur at specific molecular sites.

Keywords: dissociative electron attachment, electron transfer, taurine, thiaproline, atom-molecule collisions.

Resumo

A interacção da radiação de alta energia com o meio biológico produz diversas espécies secundárias com potencial genotóxico relevante. Estudos recentes demonstram que electrões com energia abaixo do limiar de ionização são altamente eficientes no que diz respeito à criação de quebras na estrutura do ADN e ARN. Os processos físico-quimicos que ocorrem nos primeiros instantes de interacção dos electrões não são totalmente conhecidos. É sabido que os electrões livres têm um curto tempo de vida no meio biológico, passando a existir em estados solvatados. Assim, estudos do processo de transferência de electrão são uma alternativa capaz de desvendar o papel de espécies dadoras de electrões como precursores de dano em tecido biológico.

O objectivo deste trabalho é estudar padrões de fragmentação de compostos que contêm enxofre (taurina e tiaprolina) por transferência de electrão em colisões átomo(potássio)-molécula e por captura electrónica dissociativa (CED). As medidas de CED foram realizadas na universidade de Siedlce, Polónia, no grupo da Professora Janina Kopyra através da rede COST MP1002 (Nano-scale insights in ion beam cancer therapy) num aparalho de feixes de electrões e molecular cruzados.

Os padrões de formação de fragmentos aniónicos foram obtidos por ambas as técnicas. Os resultados revelaram diferenças significativas nos dois processos, sobretudo devido à influência do ião K^+ no complexo de colisão após transferência do electrão. Para além disso, a presença do átomo de enxofre nas moléculas estudadas condiciona o processo de dissociação, demonstrando que certas reacções podem ser controladas ao substituir o enxofre em ligações específicas da molécula.

Palavras-chave: captura electrónica dissociativa, transferência de electrão, taurina, tiaprolina, colisões átomo-molécula.

Contents

List of Figures

List of Tables

Glossary

π^* π antibonding orbital.

σ^* σ antibonding orbital.

K^+_{hyper} hyperthermal potassium ion.

K^+_{ther} thermal potassium ion.

K^0_{hyper} hyperthermal potassium atom.

K^0_{ther} thermal potassium atom.

R_c crossing radius.

a.m.u. atomic mass units.

AE appearance energy.

BDE bond dissociation energy.

CEC charge exchange chamber.

CPS cationic potassium source.

DBS dipole bound state.

DEA dissociative electron attachment.

DP deflecting plates.

EA electron affinity.

ET electron transfer.

FWHM full-width at half maximum.

IE ionisation energy.

LEE low energy electron.

LTD Langmuir-Taylor detector.

LUMO lowest unoccupied molecular orbital.

m/z mass to charge ratio.

MO molecular orbital.

MTO molecular target oven.

NMR nuclear magnetic resonance.

PO potassium oven.

QMS quadrupole mass spectrometer.

SEM secondary electron multiplier.

T taurine.

TEM trochoidal electron monochromator.

TNI temporary negative ion.

TOF time-of-flight.

TP thiaproline.

VFR vibrational Feshbach resonance.

Chapter 1

Introduction

1.1 Motivation

Over the last decades, the scientific community has shown particular interest in better understanding the processes capable of damaging biological tissue, mainly those that may result in severe physiological pathologies. It soon became clear that the exposure of living tissue to ionising radiation (e.g., X-rays, γ-rays, α particles, ions, protons and electrons) may eventually cause in the long term erratic DNA replication, cellular death, cancer and mutations, as a final result of several sequenced chemical and biological mechanisms triggered in the early stages of irradiation (approximately 10^{-6} s after interaction). Indeed, the direct and indirect effects of ionising radiation are recognized as the main precursors of structural and functional cellular alterations [1].

In figure 1.1 is presented a chronological schematic representing the different stages of cell damage in biological systems, from the instant of irradiation up to a time scale of several years. The initial instants of irradiation (10^{-6} seconds) are governed by physical processes, such as excitation and ionisation, followed by physical-chemical processes that may culminate in DNA lesions. In turn, DNA damage leads to a stage where biological processes may occur and cancer may be diagnosed, reaching the medical and health sciences [2]. As such, it is fair to state that to better understand in detail certain biological effects and ultimately avoid the mentioned physiological disorders, one needs to first unravel and eventually gain control over the processes originating such chain of events, i.e. the physical and physical-chemical processes. Such knowledge may also contribute to the development of more effective and accurate treatments.

Making use of radiation's capability to damage DNA, in the medical field it is used for cancer treatments (radiotherapy, proton therapy, *etc.*), as a mean of

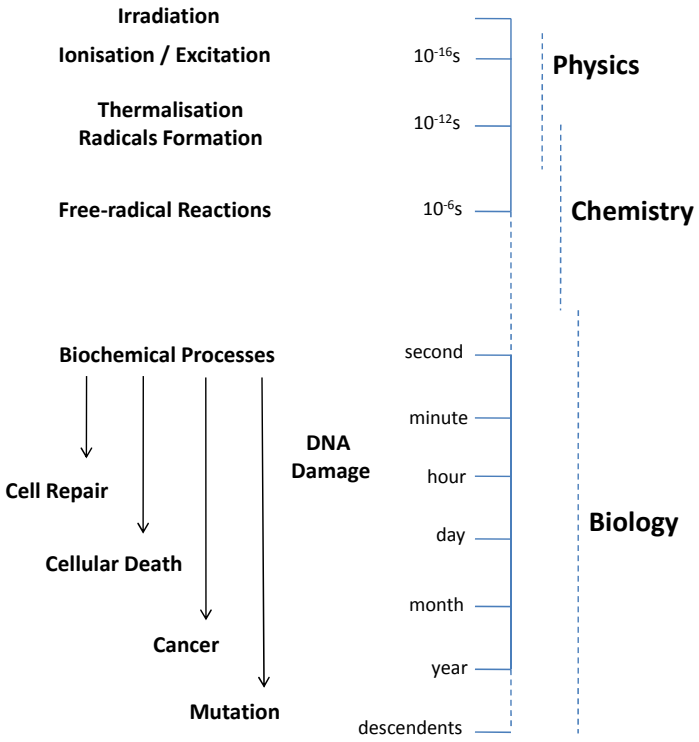

Figure 1.1: Chronological schematic of radiation effects on living beings.

destroying cancer cells. However, such therapy is also responsible for damaging the surrounding healthy tissue. In addition to the knowledge based on macroscopic evidences, the understanding of the fundamental molecular mechanisms that follow radiation impact is thus a necessary prerequisite for a more effective and controlled radiotherapy strategy.

Over the past century, great research efforts have been made to better understand the direct and indirect effects of ionising radiation interaction with biological systems, especially DNA and other cellular components. Cancer related research is driven towards the study of such mechanisms [3]. Initially, it was thought that direct ionisation and attack by hydroxyl radicals ($OH^{\bullet}$) were the main precursors for double strand breaks in DNA. However, the majority of biological effects is not related to direct interactions with the biological material, but rather with secondary species resulting upon direct irradiation [1]. Such secondary species (e.g., ions, radicals and free electrons) may be potentially more damaging than the primary radiation. Actually, the results of Brun *et al.* [4] illustrate that when the same amount of energy is deposited in DNA by photons or by low energy secondary electrons, the latter produces much more damage.

Before being thermalized, secondary low energy electrons (LEEs) can be responsible for DNA damaging by direct or indirect interaction. LEEs damage capability

is not restricted to DNA, they being also effectively capable of damaging other structures present in the cellular medium, such as proteins [5]. DNA is directly packed and ordered by proteins called histones and is also expressed by other kind of proteins called transcription factors. Due to protein's molecular and structural complexity, scientific studies rather focus on its building blocks, i.e. amino acids. Such studies intend to understand the fragmentation patterns of biomolecules upon dissociative electron attachment (DEA) processes.

Since free electrons have a short lifetime before being fully thermalized by the physiological medium, an alternative approach is to study a process that can mimic electron driven reactions in cellular medium conditions, such as the process of electron transfer (ET) from a donor atom to a biomolecule of interest. Both processes are capable of dissociating the molecule, generating multiple anionic and neutral fragments, and possibly causing its loss of functionality. Moreover, the products of the dissociation, including free radicals ($H^{\bullet}$, $OH^{\bullet}$ and $O^{\bullet}$), can in turn induce further damage.

Because DNA is the most important molecular target in radiotherapy, LEEs genotoxic effects can result in higher sensitivity of tumour cells to radiation via two strategies: (1) making DNA more sensitive to LEEs through radiosensitizers and (2) increasing the number of LEEs near the DNA. Because low energy electrons have a range of about 5 times the diameter of the DNA helix and are created in large numbers, their damage can be confined within a short distance involving few biomolecules such as DNA of cancer cells and nearby water molecules and proteins [6].

In the same line of thought, sulphur containing nucleobases are also effectively used as anticancer drugs [7]. There is, however, lack of knowledge on the consequences to these molecules upon interaction with ionising radiation. As such, the scientific community has become more aware of the importance of studies on electron driven reactions to sulphur containing biological relevant molecules, in order to further investigate the role of sulphur atoms in such processes.

This thesis addresses electron attachment and electron transfer processes to sulphur containing biological prototypes, aiming to determine fragmentation patterns through the analysis of the yielded negative ions. Within this framework, the target molecules studied in this thesis are taurine, an amino acid with various functions in the human physiology, and 4-thiaproline, a proline analogue that has been indicated as a possible anti-cancer drug. The main focus of the thesis consists of studying electron transfer to the mentioned molecules, complementing and comparing the outcome data and analysis with DEA measurements.

The core work was performed in Atomic and Molecular Collisions Laboratory (CEFITEC, Department of Physics of FCT/UNL), in a crossed beam set-up designed to perform time-of-flight (TOF) mass spectrometric studies of negative ions, resulting from electron transfer processes in atom-molecule collisions. Additionally, DEA studies have been performed in the Department of Chemistry of Siedlce University in Poland, in close collaboration with Prof. Janina Kopyra within COST action MP1002 (Nano-IBCT: Nano-scale insights in ion beam cancer therapy). In order to conduct dissociative electron attachment to biomolecules studies, an electron-molecule crossed beam apparatus was used where the yielded negative ions were detected.

1.2 Thesis Outline

This thesis starts with a background chapter where the fundamental concepts of both dissociative electron attachment and electron transfer processes are described, followed by a section summarizing the main published research work within this context. The aim of the chapter is not to provide an exhaustive description of the theory, but rather an empirical summary of the theoretical concepts essential to understand the following chapters.

In chapter 3 the experimental set-ups are thoroughly described and its working principles explained. The apparatus where the electron transfer measurements were performed is addressed on the first section of the chapter. On the following section is given a portrayal of the apparatus designed to perform dissociative electron attachment measurements.

Chapter 4 comprises the results obtained and its analysis. The chapter includes two sections assigned for the two molecules studied. In each section the results of both measurements are presented separately along with a comparative discussion.

Finally, in addition to thesis conclusions and remarks, several suggestions and future plans are presented in chapter 6.

Chapter 2

Electron Driven Reactions

2.1 Indirect Damage By Free Electrons

2.1.1 Introduction

It is now known that one of the most abundant products of living tissue irradiation with ionising radiation are LEEs. In fact, for each MeV of deposited energy in biological tissue, approximately 5×10^4 secondary electrons are produced [8]. Adding to this, the evidences show that these electrons possess an energy distribution ranging from 0 eV to ~20 eV, most of them having energies lying below the typical ionisation threshold (~10 eV) of most organic molecules [9].

Secondary electrons generated by high quanta interaction with the biological system will gradually lose kinetic energy, until reaching near 0 eV energy and becoming trapped by electrostatic interaction with the induced and permanent dipoles of the surrounding biomolecules. At this stage, i.e. within a time scale of $10^{-12}s$, electrons can be considered as being thermalized and later they become solvated [6]. Figure 2.1 represents a scheme of the thermalization process in energy, time and space scales. Aldrich *et al.* [10] studies revealed the importance of physical fast processes in biological relevant molecules, i.e. electron attachment prior to solvation.

Until recently, radiation damage was thought to be only due to direct interactions of ionising radiation. However, recent studies on low energy electrons interaction with plasmid DNA demonstrated that the role of the above mentioned direct damaging processes is less significant when compared to the damaging capability of LEEs [8, 11]. Indeed, these landmark studies show that LEEs have a resonant like-behaviour in breaking these molecules (single strand breaks and double strand breaks), as well as loss of supercoiled helicity [8], at energies lower

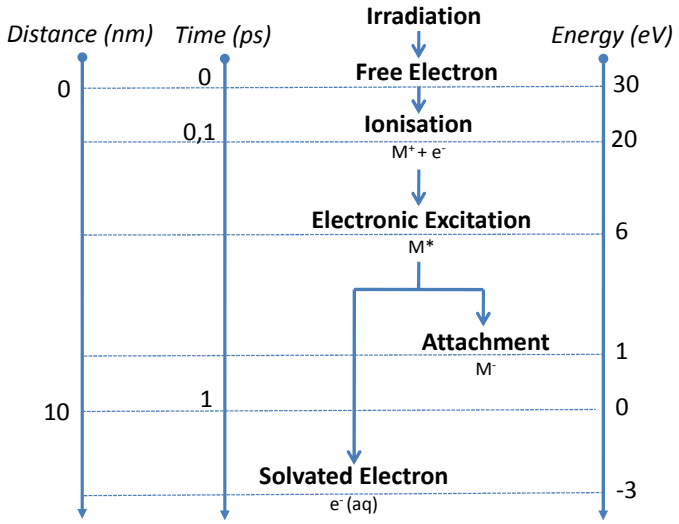

Figure 2.1: Thermalization of electrons after being created by interaction of high energy quanta with the physiological medium: energy, time and space scales [1]

than the ionisation threshold (~10 eV) and even at energies lower than excitation energies (~3 eV) [12]. Boudaiffa *et al.* [8] and Lehnert *et al.* [13] even suggest that 70% of the DNA damage is related to secondary low energy electrons, the remaining 30% being related to direct deposition of energy. By demonstrating that electron capture by DNA composing molecules is the main cause for the formation of single and double strand breaks in DNA chains within this energy range, Boudaiffa *et al.* [8] changed the paradigm of radiation induced damage, since a new set of natural processes has to be taken into account.

Following Sanche's work [8], several other dissociative electron attachment and theoretical studies were conducted, focusing mostly on different other biological relevant molecules such as nucleotides, sugar units and amino acids.

Considering the interaction of a low energy electron with a molecule under single collision conditions, electron attachment can be seen as a resonant scattering process which, as opposed to direct scattering, occurs if the incoming electron is trapped for a certain period of time (much longer than its normal transit time) in the vicinity of the molecule, forming a temporary negative ion (TNI). The capture only occurs for electrons with the appropriate energy [9]. Besides, when the energy of the electron after being detached equals its incident energy the scattering is elastic, otherwise is called resonant inelastic scattering.

The resulting molecular anion can react via the following channels:

$$e^- + AB \rightarrow (AB^-)^* \rightarrow (AB)^- + hv \tag{2.1}$$

$$(AB^-)^* \rightarrow (AB)^* + e^- \tag{2.2}$$

$$(AB^-)^* \rightarrow A + B^- or A^- + B \tag{2.3}$$

Where e^- represents the incident electron and AB a generic molecule.

Reaction 2.1 represents radiative stabilization of the TNI to its stable ground state, being capable of confining the extra electron. This reaction implies release of the excess internal energy by photon emission. Since radiate lifetimes are on the order of $10^{-9} - 10^{-8}$ s, which is significantly higher than the latter processes, this mechanism will not be able to compete with the other two presented channels, unless some external influence confines the electron in the vicinity of the molecule long enough for the anion to stabilize.

Another reaction channel, depicted in equation 2.2, refers to autodetachment of the extra electron from the TNI. As mentioned before, this mechanism can be both elastic and inelastic. In the latter case, the resulting molecule is left in an electronic or vibrational excited state.

The TNI lifetime varies on a large scale, depending on the size of the molecule and the resonance energy. According to Heisenberg's uncertainty principle, the lifetime of a TNI is related to the energy width given by:

$$\Gamma \approx \frac{\hbar}{\tau} \tag{2.4}$$

Where Γ is the energy width of the resonance, $\hbar$ the Planck constant and τ the lifetime of the anionic state.

Finally, equation 2.3 represents a dissociative electron attachment process which, as written before, is believed to be the main responsible for most of the damage to biological systems. This mechanism consists on fragmentation of the molecular anion producing an anionic fragment and one or more neutral fragments. The dissociation itself is due to the instability created by the repulsive behaviour inherent to the attached electron, which is usually captured into a lowest unoccupied molecular orbital (LUMO) with antibonding character. This process competes directly with autodetachment. Furthermore, having a resonant behaviour, DEA only occurs for incident electrons with a specific energy. Adding to this selective characteristic, it has been recently shown that such process can

be also site and bond selective, i.e. the process can selectively occur depending if the electron is captured into specific regions of the molecule and specific chemical bonds [14, 15, 16, 17].

On the other hand, one should note that in addition to direct damage to cellular constituents, low energy electrons also have an indirect role. Indeed, secondary electrons may interact with other molecules present in the surrounding environment and generate reactive species (ions, excited molecules and free radicals), which in turn are known to have the capability to efficiently damage DNA. Given that cells are 70% composed of water, radicals $H^{\bullet}$, $OH^{\bullet}$ and $O^{\bullet}$, products of H_2O radiolysis, are proven examples of such significant role.

2.1.2 Dissociative Electron Attachment (DEA)

The process of dissociative electron attachment described in equation 2.3 can be pictured in a Born-Oppenheimer potential energy diagram, as depicted in figure 2.2. Such curves are only applicable to diatomic molecules, while for polyatomic molecules they represent two-dimensional cuts through hyperdimensional surfaces along a reaction coordinate.

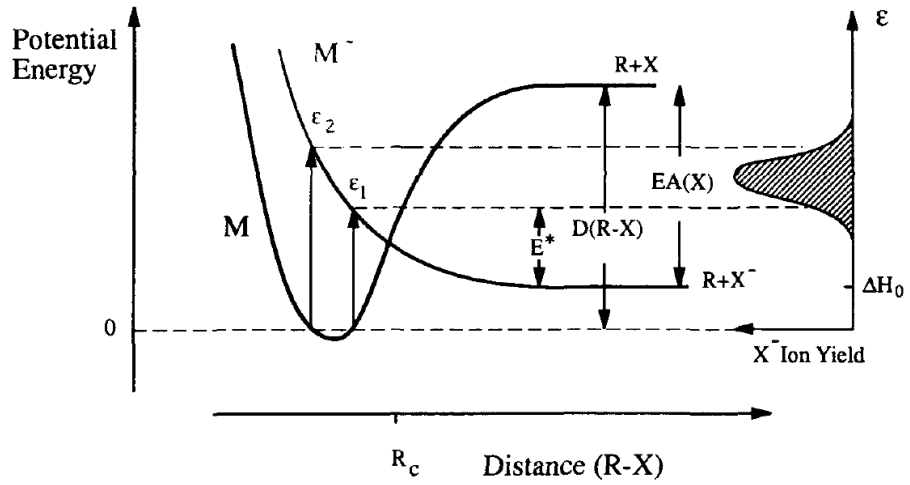

Figure 2.2: Born-Oppenheimer potential energy diagram associated with electron attachment and subsequent electronic dissociation. Adapted from [9].

The capture of an electron into a virtual molecular orbital (MO) allows a bond rupture if the binding energy of the extra electron (electron affinity) is high enough

to compensate the bond dissociation energy, D(R-X). Hence, the lowest energy limit for DEA is given by:

$$\Delta H_0 = D(R - X) - EA(X) \tag{2.5}$$

Considering electronic transitions, one can make the approximation that they are most likely to occur without changes in the position of the nuclei involved. This approximation is known as the Franck-Condon principle and the transitions involved are called vertical transitions [18]. According to the Franck-Condon principle, transitions from the continuum state ($M + e^-(r \to \infty)$) to the temporary negative ion (M^-) are only possible within the energy range between ϵ_1 and ϵ_2 (figure 2.2).

Autodetachment can occur for internuclear distances smaller than R_c, which is the crossing point of the two potential energy curves. For radius longer than R_c the extra electron is bound to fragment X to a degree that autodetachment of M^- is no longer possible.

On the right-hand side of figure 2.2 is shown the ion yield curve as a function of the incident electron energy (ϵ). The excess energy is represented in the same figure as E^*, as well as the electron affinity (EA).

2.1.3 Dynamics of anion formation

In order for dissociation to occur, the extra electron must be somehow trapped to prevent immediate autodetachment. This subsection addresses the electronic configuration of the temporary negative ions in resonant electron attachment.

If the electron is captured without changing the electronic configuration of the target molecule, i.e. if the extra electron is added into one of the unoccupied virtual MOs, one speaks of a single particle (1p) resonance. On the other hand, if the electron attachment is accompanied by an electronic excitation of the molecule, meaning that two electrons will be in normally unoccupied MOs, the resonance is called core excited or two particle one hole (2p-1h) resonance.

If the energy of the core excited resonance lies above that of the excited neutral (the parent electronic state), the resonance is called open channel core excited resonance. However, if it lies below, one refers to a closed channel or Feshbach resonance. The latter implies a much longer lifetime of the anion, since the parent excited state cannot be reached any more.

The other mechanism which is valid for single particle and open channel core excited resonances pertains to the trapping of the extra electron by the shape of the

effective interaction potential between the electron and the neutral molecule. For that reason, such resonances are called shape resonances. The effective interaction potential is the combination between the charge-induced polarization potential for long-range interaction and the repulsive centrifugal potential at shorter distances, where electron-electron repulsion dominates. Such combination results in a potential barrier where an electron can eventually be trapped. However, these resonances have short lifetimes since the electron can escape by tunnelling through the barrier.

At low energies vibrational Feshbach resonances (VFR) can occur. This trapping mechanism is likely to take place in molecules having a very large dipole moment ($> 2.5D$) leading to a long-range attractive interaction. The extra electron becomes trapped in a very diffuse orbital whose dimensions are very large when compared to the size of the resulting ion core (Rydberg-like orbital), on the positive side of the dipole, resulting in an anion with a geometry similar to the neutral. Hence, the anionic state is also called dipole bound state (DBS) [19]. In free electron attachment, these states are only accessible if release of the excess energy through internal vibrational redistribution takes place. Such resonance can serve as a "doorway" for dissociation if it is coupled to a dissociative valence state.

While shape resonances usually occur at energies below 4 eV, core excited resonances can occur from 4 to 10 eV.

Figure 2.3 summarizes the possible resonances in terms of formation energy.

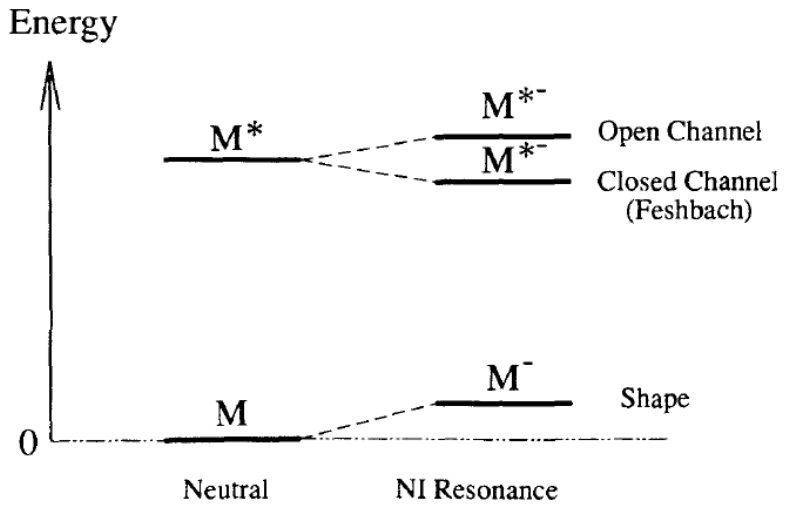

Figure 2.3: Classification of resonances. NI - Negative ion. Adapted from [9].

2.2 Damage By Electron Transfer

2.2.1 Introduction

Over the past few years, studies on low energy electrons interaction with biologically relevant molecules in the gas-phase have increasingly come under scrutiny. Such studies were mainly driven by the discovery of the capability of secondary electrons to induce single and double strand brakes to DNA. However, free electron attachment processes may not be sufficient to accurately describe dissociation reactions within the physiological environment. As mentioned before, once generated in the physiological medium, the LEEs will not act as free electrons after a short period of time, but should be rather treated as being in a bound state, namely solvated in water. In fact, the solvated electron is an important species with high chemical reactivity and consequent short lifetime (like most free radials). Being the simplest electron "donor", its reactions correspond to electron transfer mechanism [20].

Given this context, further investigation on electron transfer of "bound" electrons to biological relevant molecules (as in atom-molecule collisions) can provide additional information not reached through DEA studies. In addition, the presence of the cation created after the electron transfer by the electron "donor", can change the accessed channels and fragmentation patterns of the molecule in study. For these reasons, electron transfer studies may be an alternative approach to study free electron reactions, when aiming to simulate electron driven dissociation reactions within the cellular medium.

In atom-molecule collisions a neutral atom with a weakly bound electron (A) has the role of electron donor. Reaching a certain distance from the relevant molecule, A transfers its valence electron to the molecular target (BC) yielding, much like in the electron attachment process, a transient negative ion. After that, several pathways may take place in what concerns TNI, from which the following are the most likely to occur:

$$A + BC \rightarrow A^+ + (BC^-)^* \rightarrow A^+ + (BC^-); \text{(Non-dissociative ionisation)} \quad (2.6)$$

$$A^+ + (BC^-)^* \rightarrow A^+ + B^- + C; \text{(Dissociative ionisation)} \quad (2.7)$$

$$A^+ + (BC^-)^* \rightarrow (AB)^+ + C^-; \text{(Associative chemionisation)} \quad (2.8)$$

Equation 2.6 represents the pathway where the relevant molecule is able to form the parent anion. Pathway 2.7 depicts the fragmentation of the TNI, much like in the DEA case. Nevertheless, it is worth noting that despite accessing the same resonance as in DEA, the TNI obtained in electron transfer may decay through different pathways and thus yield different fragments. Reaction 2.8 represents the capture of an atomic element from the molecule by the electron donor (usually a proton).

As in DEA processes, electron transfer may be also described dividing the mechanism in two different stages: first the donor projectile (A) must undergo ionisation in the vicinity of the electron acceptor (BC); then, the ejected electron must be captured by the target molecule, leading to the formation of the TNI.

The described process depends on two important physical properties. One is the electron affinity (EA) of the target molecule and the other is the ionisation energy (IE) of the projectile electron donor atom. EA is defined as the amount of energy needed for the electron to detach, i.e. the ability of an atom or molecule to thermodynamically form a stable TNI. Therefore, electron affinity is given by the difference between a neutral atom or molecule's ground state energy and that of its corresponding anion, as written in the following equation:

$$EA(BC) = E(BC) - E(BC^-) \tag{2.9}$$

The endoergicity of the electron transfer process is determined by the ionisation energy of the "donor" atom and the electron affinity of the target molecule (cf. equation 2.10).

$$\Delta E = IE(A) - EA(BC) \tag{2.10}$$

Where ΔE is the reaction energy. If the ionisation energy of the atom is higher than the electron affinity of the target molecule, then the reaction is endothermic.

As opposed to electron attachment, associated to electron transfer processes in atom-molecule collisions arises the possibility for excess internal energy to be transferred to positive species, since a third body (A^+) is present. Following the comparison to electron attachment, it has been shown that atom-molecule collisions allow the formation of a stable parent anion (BC^-) [21], possibly due to a coulomb interaction between the positive ion (A^+) and the TNI. Such process can also access different reaction channels and yield different fragments from DEA.

In this thesis electron transfer studies of "bound" electrons to biological relevant molecules will be performed. In order to do so, a crossed beam set-up comprising a neutral potassium atoms beam and a target molecule effusive beam was used to

investigate negative ion formation. Neutral potassium atoms are used due to their low ionisation energies (IE(K) = 4.34 eV). Although neutral potassium atoms do not exist in the physiological medium, they provide a key insight on the effects of charge carriers in the degradation of relevant biomolecules.

2.2.2 Atom-Atom Collisions

Two different processes can occur from collisions between two neutral atoms in their ground state: elastic scattering and inelastic scattering. The first implies the conservation of the systems' total kinetic energy, regardless of the kinetic energy transfer from one atom to the other, where both species are kept neutral. On the other hand, conservation of total kinetic energy is not observed in inelastic scattering, where the involved atoms can be left in different electronic states from before the interaction. This thesis addresses a particular mechanism of inelastic scattering, in which an electron is transferred from one atom to the other with possible electronic excitation of the electron acceptor.

The electron transfer process may be characterized through the following reaction, where A represents the electron donor atom, B the electron acceptor atom and * means excited electronic state:

$$A + B \rightarrow A^{+} + (B^{-})^{*} \tag{2.11}$$

The interaction between two particles can be described in quantum mechanics as a system that obeys the time-dependent Schrödinger equation [22]:

$$H\Psi(r,R) = i\hbar\left(\frac{d\Psi(r,R)}{dt}\right) \tag{2.12}$$

Where Ψ is the total wavefunction, r represents the electronic coordinates, R represents the nuclear coordinates and H is the Hamiltonian operator, which in turn can be written as

$$H = T_n + T_e + V \tag{2.13}$$

In which T_n and T_e represent the nuclei and electrons kinetic energy operators respectively, and V is the sum of all potentials between all of the intervening particles of the system.

It is not possible to solve the Schrödinger equation considering all viable interactions included in 2.13. As such, the solution of 2.12 can only be achieved by means of approximations, the first being the Born-Oppenheimer approximation which consists of separating the motion of the nuclei from the motion of the

electrons. Since the mass of a proton is 1836 times larger than that of an electron, electrons in an atom will move at much higher speed than the nucleus. When the nuclei make small changes in their relative position, the electrons almost instantaneously adjust to the new set of nuclear positions. Thus, the nuclei motion is considered to have no influence on the electronic motion.

On one hand, the Born-Oppenheimer approximation allows for considering the motion of the nuclei as a classical trajectory ($R(t)$), in which they move as a function of the final electronic state. Furthermore, it is valid to consider the nuclei fixed when studying the behaviour of the electrons. This corresponds to neglect the influence of the operator T_n.

The subsequent step lies in considering that the nuclei move slowly, inducing slow modifications in the potential felt by the electrons. In this context, the electrons' dynamic state will adiabatically accompany the motion of the nuclei and the Born-Oppenheimer approximation is still valid. This means that as long as $R(t)$ does not vary rapidly, we can adapt the fixed-nuclei solution for the Schrödinger equation (from the Born-Oppenheimer approximation) to a time-dependent solution. In other words, it is possible to describe a dynamic situation in which the nuclei coordinates change over time but allow the electrons to reach their equilibrium positions.

Electron transfer in atom-atom collisions is, in general, mediated through the crossing of adiabatic potential energy surfaces of the covalent ($A + B$) and ionic ($A^+ + B^-$) states (equation 2.11). The switch between ionic and covalent configurations occurs if the adiabatic principle is valid, i.e. if the particles approach each other slowly. If the internuclear distance changes rapidly, the valence electron does not have sufficient time to jump from one atom to the other. In that case the system remains in the same electronic configuration [23].

The non-crossing rule states that potential energy curves corresponding to electronic states with the same symmetry cannot cross. From that, if two adiabatic states with the same symmetry come together, the respective wave functions will change their character. However, if the particles come across each other along one of these states (ionic or covalent) with sufficiently high velocity, the time spent in the avoided crossing region could be short for the electrons to adjust their positions. This means that the system violates the non-crossing rule and moves, in this region, along a non-adiabatic (diabatic) potential curve [24].

In summary, in the context of atom-atom scattering, non-adiabatic transitions between adiabatic states will mean the transfer of an electron from one atom to the other, designated by ion-pair formation [22, 24, 25].

The probability of a non-adiabatic transition (electron transfer) between two states has been calculated by Landau, Zener and Stueckelberg by solving the time-dependent Schrödinger equation for a simple one dimensional, two state system. This model assumes that the transition only occurs in a strict region around the crossing radius (R_c), where the radial velocity is constant (linear trajectory) and equivalent for both electronic states. As such, the Landau-Zener formula for the non-adiabatic transition is given by [24]

$$p = exp\left(-\frac{v^*}{v_r}\right) = exp\left(-\frac{v^*}{v}\left(1-\frac{b^2}{R_c^2}\right)^{-1/2}\right) \tag{2.14}$$

Where v^* is the reduced velocity and b is the impact parameter, in Å.

To better illustrate the ion-pair formation process from the charge transfer point of view, the analysis of the curve crossing is shown in figure 2.4.

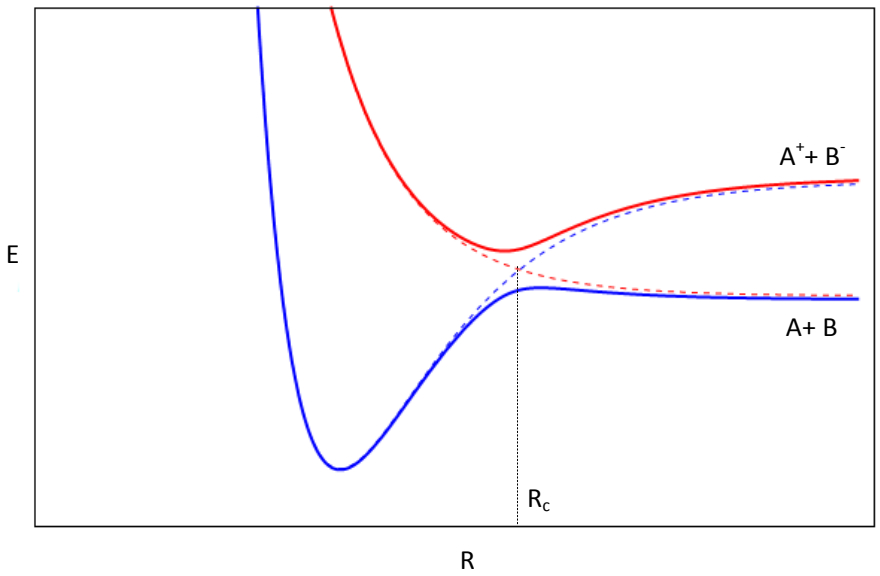

Figure 2.4: Adiabatic and non-adiabatic potential energy curves for a general atom-atom collision, as a function of the internuclear distance (R). Full curves represent the adiabatic ionic (red) and covalent (blue) states. Dashed curves correspond to the non-adiabatic ionic (red) and covalent (blue) states. Adapted from [26].

It is clear from the curves representation that the non-adiabatic and adiabatic states are similar for internuclear distances much larger than the crossing radius, where an avoided crossing between the adiabatic states is observed. The separation between the covalent and ionic potentials at infinite A-B internuclear distance is given by the endoergicity value (equation 2.10).

Making the approximation of considering that the crossing radius is large, it is possible to neglect the Van der Waals and induction forces, thereby making the

covalent potential zero and the ionic potential can be given by a pure coulombic potential. Such consideration leads to R_c being approximated by:

$$R_c = \frac{e^2}{\Delta E} = \frac{14.41}{IE(A) - EA(B)} \tag{2.15}$$

With R_c in Å and ΔE in eV.

Until now, in this discussion a single crossing point has been considered. However, in an atom-atom collision, for a given impact parameter $b < R_c$, two crossing points will appear. Considering a straight line trajectory, figure 2.5 illustrates the possible collision trajectories upon interaction.

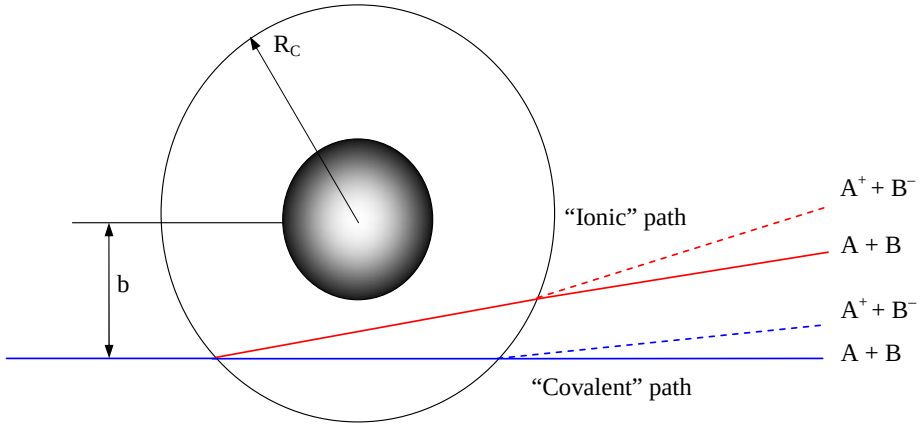

Figure 2.5: Schematic of atom-atom scattering with b representing the impact parameter, the shaded area representing the repulsive part of the potential. Red curves represent the ionic path and blue curves represent the covalent trajectory. Adapted from [26].

According to figure 2.5 there will be four possible processes. If the electron is transferred at the first crossing the coulombic interaction between the formed ions will generate a deflection in the trajectory of the cation. Even if the electron is transferred back to the first electron donor (now cation) at the second crossing, the deflection is still significant. On the other hand, if no electron transfer occurs at the first crossing, the trajectory of the electron donor will not be significantly affected, despite of a possible charge transfer at the second crossing. If the electron jump occurs at the first crossing, the scattering happens along the "ionic" path. If no electron transfer occurs at the first crossing, the scattering happens along the "covalent" path. Both ionic and covalent states can result from the so-called "covalent" and "ionic" paths.

For ion-pair formation, the electron jump must occur only at the first or at the second crossing, which only happens within two of the four trajectories (inelastic scattering). If the electron transfer does not occur or if it occurs at both crossings, no ion-pair formation will happen (elastic scattering).

On a relevant note, to better understand the electron transfer process in atom-atom collisions, it is helpful to follow the potential curves illustrated in figure 2.4 together with the more pictorial representation of the process presented in figure 2.5. In fact, starting from the right of figure 2.4, one can simulate the neutral acceptor and electron donor atoms coming together (along the blue line) until they reach the first crossing point, where the electron can be transferred. The second crossing point is simulated following the curves from left to right.

2.2.3 Atom-Molecule Collisions

Although some of the principles discussed in section 2.2.2 still apply to atom-molecule collisions, to describe the latter system a much more elaborate analysis is required, due mainly to the increased structural complexity of the molecular target. New processes have to be considered when studying such a collision system, namely rotational, vibrational and electronic excitation of the electron acceptor (molecule), as well as collision-induced dissociation, or a combination of all the aforementioned processes.

The description of atom-molecule collisions is interpreted by means of multi-dimensional potential hypersurfaces, in which numerous nuclear coordinates of the molecule have to be taken into account, in contrast with the uni-dimensional potential energy curves derived from the collision between atoms. For interpretation purposes, the time period associated with rotational and vibrational movements of the molecule have to be considered in the analysis. The time it takes for a molecule to rotate is relatively long when compared with the collision time and therefore may be neglected, i.e. considered frozen. Nevertheless, the vibrational time is in the same order of magnitude of the collision time, meaning that vibrational effects have to be considered in the collision process [24].

Some models have been developed to electronically describe inelastic collisions between atoms and diatomic molecules [23]. However, such models are not valid for polyatomic molecules where, again, there is a significant number of processes that can occur. In fact, the mentioned models do not apply to the molecules studied throughout this thesis and therefore it is not convenient to make use of them.

Despite the complexity of the theoretical models, it is possible to describe the

electron transfer process in these collisional systems on a more qualitative perspective. Indeed, by analysing and complementing the electron transfer data with electron scattering, quantum mechanical calculations and dissociative electron attachment profiles, it is possible to obtain relevant information about the general behaviour of such process.

As mentioned before, dissociative electron attachment consists of the capture of a free electron by the target molecule resulting in a TNI that may decay through different reaction pathways. Such mechanism may be compared with what occurs in atom-molecule collisions, bearing in mind two major differences: in the latter process the electron is initially in a "bound" state; and the capture of an electron will result in the formation of a positive ion species in the vicinity of the recently generated anionic molecular target. The aforementioned differences will influence the fragmentation pathways of the TNI when comparing DEA with electron transfer in atom-molecule collisions.

The electron transfer mechanism may be generically described as follows: on a first step, the "bound" electron is detached from the electron donor projectile; on a second step the electron is captured by the electron acceptor target molecule. From this rationale, one can state that electron capture from a molecule is a resonant process, much like for DEA, and thus only certain energy losses from the system can culminate in electron transfer. This means that if the available energy of the system is high enough for the anionic state of the molecule to be accessed, this state will be formed [27].

The available energy is defined as the kinetic energy of the electron donor in the centre-of-mass framework, considering its ionisation energy:

$$E_a = \frac{m_{tm}}{m_{tm} + m_K} \cdot \alpha \cdot E_{lab} - IE \tag{2.16}$$

With E_a being the available energy (in eV), m_{tm} the target molecule's mass, m_K the projectile mass, E_{lab} is the kinetic energy of the projectile relative to the lab frame defined as the voltage applied to the potassium ion source, α is an experimental correction factor and IE is the ionisation energy of the electron-donating projectile, which in the present experiment was neutral potassium atom. The potassium ionisation energy is 4.34 eV.

The experimental parameter (α) is adimensional (approximately 0.89) and arises from the need to correct the influence of the non-linear acceleration field of the potassium source on the effective available kinetic energy of the projectile. Studies on this subject have been reported [28] and, in addition, all measurements

assuming this formula appear to yield available energy values according to what is expected by DEA.

A resonant anionic state can be accessed if the available energy (E_a) of the projectile is higher than the energy of such state. In contrast, anionic resonance states with energies above E_a cannot be accessed. Through this rationale, by changing the kinetic energy of the potassium beam to values where E_a is below certain resonant anionic states, it has been shown for several molecules that the resonances accessed through electron transfer appear to be the same as in DEA, despite the fragments yield being different [27]. Although E_a may be higher than a certain resonance, the electron is transferred with the energy equal to the accessed resonant anionic state.

As pointed before in this section, the presence of the electron donor in the vicinity of the resulting molecular anion has a critical influence on the reaction pathway after electron transfer. An example of the influence of this temporary reaction complex in the fragmentation channels pertains to the nitromethane (CH_3NO_2) studies. The parent anion ($CH_3NO_2^-$) was observed in electron transfer with potassium atoms measurements, whereas it was was not reported in DEA studies. Such difference is justified by the presence of the cationic potassium generated after transferring the electron, allowing enough time for the parent anion to stabilize into a stable geometry [29].

Despite this assumption, it is not totally clear the exact way the mentioned reaction works. The accepted empirical reasoning is that, after electron transfer, a chemical complex is formed that interacts through a coulombic potential. Such complex will probably suppress the rejection (autodetachment) of the extra electron from the molecular anion. That is, the competition between autodetachment and formation of the parent anion favours the latter, in clear contrast with what happens in the DEA case.

Also due to the presence of the cationic species, electronic states with positive electron affinity can be accessed through electron transfer, as opposed to DEA. In order for the electron affinity to be positive, the ground state energy of a neutral atom or molecule has to be higher than that of its corresponding anion (cf. equation 2.9). This means that the transition from the first electronic state to the latter is exothermic and therefore can only happen in the presence of a third body as a vehicle to release the excess energy. This is true in the electron transfer case, where a coulombic complex is formed, and not achievable in DEA in single collision conditions. In DEA the excess energy can be released by photon emission, however the lifetime of such process is too long and does not compete with dissociation or

autodetachment (section 2.1.1).

2.3 State Of The Art

As mentioned along the previous chapters, Sanche's seminal studies [8, 11] showing that low energy electrons can efficiently damage DNA by inducing resonant single and double strand breaks, motivated field-related investigators to better understand electron driven reactions in the physiological medium. Indeed, several experimental and theoretical DEA studies with segments and building blocks of DNA and RNA molecules have been reported, in the gas-phase and deposited as thin films [2, 30, 31, 32, 33]. Investigation of electron attachment process to phosporic acid esters, in order to simulate the behaviour of the phosphate group in DNA [34], and to the nucleotide deoxycytidine monophosphate (dCMP) [35] are two good examples of DEA studies aiming to reveal the LEEs induced damage to DNA. Furthermore, formation of negative ions from electron attachment to other biological relevant molecules, such as amino acids, have been studied [36, 37, 38].

Site- and bond-selective cleavage upon DEA was reported for the nucleobases thymine an uracil [14, 17, 39], ribose [19], amino acids [40] and various other biomolecules. In the case of pyrimidine bases thymine and uracil, the loss of an hydrogen atom is site- and bond-selective from the N1 position of the ring for electrons with energies close to 1 eV, whereas electrons with energies between 1 eV and 3 eV are required to induce the loss of one hydrogen atom from the N3 position of the ring. These experiments revealed that electron-induced dissociation can be a controlled process, i.e. by tuning the initial electron energy one can control specific chemical reactions in DEA.

Aiming to better mimic electron driven reactions in the physiological medium, electron transfer in atom-molecule collision measurements were pursued. In fact, following the same path and reasoning taken for electron attachment experiments, research on electron transfer to pyrimidine nucleobases [41], sugar units present in the DNA and RNA chains (D-ribose and an analogue THF) [42, 43], amino acids valine and alanine [44], and other biomolecules was performed. Remarkable site and bond selectivity has also been shown [41] in thymine and uracil studies: by tuning the collision energy of the projectile potassium beam, H^- abstraction results from N-H bonds rather than from C-H ones, and from N1 site versus N3. A joint study has also revealed the structure NCO^- as a key fragment upon dissociative electron attachment and electron transfer to pyrimidine nucleobases, having these processes a pronounced site selectivity. Ferreira da Silva *et al.* [45]

proposed both site selectivity and a chain of reactions composing a slow decay process as possible causes underlying the formation of the referred anion.

Chemoradiation therapy is gradually becoming a dominant cancer treatment. When using both chemotherapy simultaneously with radiotherapy, lower doses are required compared to single radiotherapy treatments. Such concomitant therapy involves a radiosensitizer that will improve DNA damage upon radiation interaction, increasing cancer cells death rate. Halouracils are a good example of radiosensitizers. Such molecules are uracil analogues where the methyl group in the position C5 is replaced by an halogen atom. Electron transfer studies to halouracils (5-chlorouracil and 5-fluorouracil) yielded several anionic fragments that require the ring to break, resulting in its function loss,proving its enhanced "sensitivity" to radiation damage [46].

The role of sulphur atoms in electron driven reactions to biological molecules still need to be unravelled. Naturally sulphur containing amino acids, such as cysteine and methionine, have already been subjected to DEA studies [47, 48]. On a recently published article [49], the authors show results of DEA to gas-phase thiothymine, which is a sulphur containing analogue of thymine, and suggest that the sulphur atom plays a key role on the dissociation process. Making use of experimental data and theoretical computational methods, they were able to conclude that the sulphur atom within this molecule strongly controls the fragmentation pathways. The most intense products of the dissociation process comprise the sulphur atom (S^-, SCN^- and $[M-S]^-$, where M represents the intact molecule), suggesting that the resonances are localized in the C-S group. In the same line of thought, electron attachment to sulphur containing analogue of uracil (2-thiouracil) revealed that most of the damage is localised at the sulphur site, the main yielded fragment being the thiocyanate, SCN^- [50].

These results show that certain reactions can be controlled by placing a sulphur atom at a specific site within nucleobases. Hence, they represent a first step to understand the sulphur containing molecules role on further inducing cellular damage and its potential application in chemoradiation therapy.

The work performed in this thesis comprises measurements with two sulphur containing molecular targets: taurine (2-amino-ethanesulfonic acid) and thiaproline (L-4-thiazolidinecarboxylic acid).

Taurine is the most abundant intracellular amino acid in the human body. Higher concentrations of this amino acid are found in tissues that are prone to generate free radicals, such as retina, brain, central nervous system and heart [51]. It has a unique chemical structure that implies important physiological

functions: taurine promotes bile flow and increases bile acid production; in the central nervous system taurine has the role of neurotransmitter and acts as neuroprotective agent; it has positive cardiovascular antiarrhythmic effects; and its deficiency leads to retinal degeneration. Furthermore, taurine has therapeutic applications. In fact, it may inhibit nerve stimulation and has been reported to control motor tics, such as uncontrollable facial twitches [52], and it has been suggested that taurine may act as an antioxidant.

Thiaproline is a proline analogue in which a carbon atom from the amino acid ring is substituted by a sulfur atom. This fact alone represents an interesting research path when aiming to better understand the role of sulfur atoms, by comparing thiaproline and proline data. Thiaproline has been pointed out has a cancer treatment drug found to act on the cell membrane of tumour cells [53]. A japanese research group has shown that thiaproline prevents carcinogenesis [54]. In addition, it was proposed that thiaproline inhibits proline incorporation into polypeptides in protein synthesizing systems [55].

Chapter 3

Experimental Set-ups

This chapter is devoted to the characterization of the two experimental set-ups used throughout the work performed in this thesis. The bulk of the work pertains to the studies on electron transfer in collisions between neutral potassium atoms and biomolecules, and was performed in Atomic and Molecular Collisions Laboratory, CEFITEC. The crossed beam set-up designed to perform such studies is described in the first section.

Part of the research studies were performed in the Department of Chemistry of Siedlce University in Poland, where dissociative electron attachment measurements were conducted, making use of an electron-molecule crossed beam apparatus described in the second section of the present chapter.

3.1 Electron Transfer Experimental Set-up

3.1.1 Apparatus Overview

A scheme of the experimental device is presented in figure 3.1. The apparatus can be divided into two main regions, which are set in two high vacuum chambers differentially pumped through diffusion pumps, reaching base pressures of the order of 10^{-5} Pa (10^{-7} mbar). The chambers communicate through an aperture valve.

In the potassium chamber (first region), a hyperthermal neutral potassium beam is created by resonant charge exchange, with an adjustable kinetic energy ranging from 10 to 300 eV. The accelerated potassium beam enters the collision chamber (second region) where it is monitored by a Langmuir-Taylor detector, and reaches the collision region, which corresponds to the chamber's geometrical center. Also in this chamber, an effusive beam of the target molecule, orthogonal

to the potassium beam, is created in an oven (called molecular target oven) where liquid, gas and solid samples are admitted. Both beams enter the collision region through two different collimation slits: an horizontal 5×0.5 mm slit is placed in the potassium beam path, whereas an aperture with 1 mm diameter is placed in the molecular beam axis.

In addition to the molecular target oven and the Langmuir-Taylor detector, the second region comprises the extraction system of the TOF mass spectrometer. The collision region consists of two parallel plates 1.2 cm apart and equally distanced to the collision plane. The anionic fragments resulting from electron transfer in potassium-molecule collisions are extracted by applying an electric field normal to the collision plane. The fragments pass through an Einzel lens system designed to focus the ions before entering the time-of-flight tube towards the channeltron detector.

In the second chamber a set of heating lamps is installed to both avoid the condensation of samples on the chamber's walls and to facilitate the baking of the chamber. Typical working pressures are in order of 6×10^{-4} Pa (6×10^{-6} mbar), depending on the sample. Both the TOF tube and the liquid and gas samples inlet system tubes are wrapped with heating bands to avoid condensation of the samples on the respective walls.

3.1.2 Projectile Beam

The accelerated neutral potassium beam is obtained through a process based on the collision between a hyperthermal potassium ion (K^+_{hyper}) and a thermal potassium atom (K^0_{ther}), resulting in an electron jump from the second to the first, i.e. they undergo resonant charge exchange. Being a resonant process, the hyperthermal potassium ion becomes neutral and no kinetic energy is lost. Such process can be described as follows:

$$K^+_{hyper} + K^0_{ther} \rightarrow K^0_{hyper} + K^+_{ther} \tag{3.1}$$

Where the products of the reaction are the desired hyperthermal potassium atom (K^0_{hyper}) and the thermal potassium ion (K^+_{ther}).

The charge exchange source used and its working principle is pictorially shown in figure 3.2. A cationic potassium source is placed 2 mm next to the entrance slit of the charge exchange oven. Solid potassium is placed in the potassium oven, where it is heated and vaporized diffusing into the connected charge exchange oven. The potassium oven is heated by two cartridge heaters to approximately 393 K, and controlled by two PT100 resistors. The temperature of the charge exchange

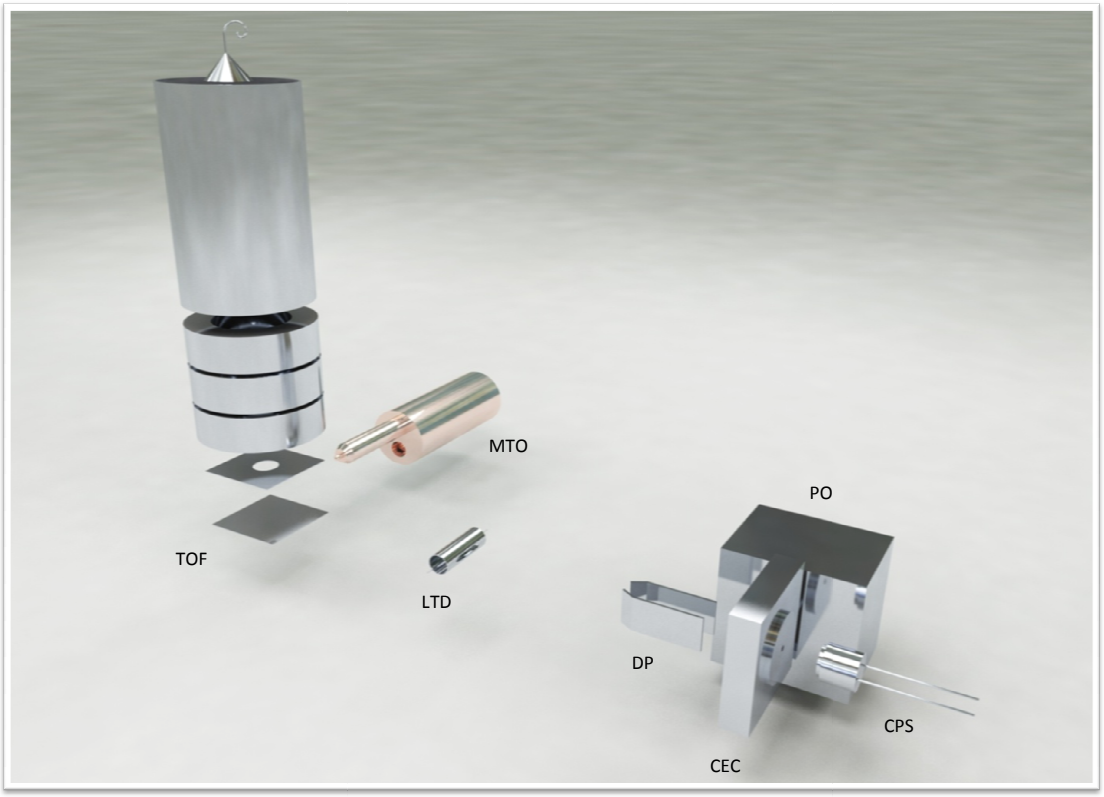

Figure 3.1: Schematic of the electron transfer experimental device. PO: Potassium oven, CEC: Charge exchange chamber, CPS: Cationic potassium source, DP: Deflecting plates, LTD: Langmuir-Taylor detector, MTO: Molecular target oven, TOF: TOF mass spectrometer. Adapted from [26].

oven is maintained 20 K higher than the potassium oven to avoid condensation inside and in the entrance and exit collimation slits.

The potassium ions are pushed towards the charge exchange oven with the desired energy by applying an acceleration voltage between the ion source and the oven, where the neutral potassium lies. The ions that enter the oven go through resonant charge exchange and become neutral (K^0_{hyper}).

The resulting beam is composed mainly of hyperthermal potassium atoms that enter the collision chamber with a kinetic energy given by the applied acceleration voltage. However, since only a fraction of the potassium ions undergo resonant charge exchange, exiting the charge exchange oven one finds hyperthermal potassium ions (K^+_{hyper}), which therefore must be removed. With that purpose, a pair of deflecting plates are placed (10 mm) at the exit slit. A positive voltage is applied to one of the plates, repelling the ions towards the other plate, parallel to the first and connected to ground potential or an electrometer. It is possible to monitor the potassium ions production rate by measuring the ionic current in the deflecting

plates. Such current also gives an indication of the charge exchange efficiency, which is related to the potassium vapour density in the charge exchange oven. The voltage applied to the deflecting plate varies according to the beam kinetic energy (optimal values were tested [26]). The measured ion currents increase with increasing beam kinetic energies and are in the order of 1-100 nA.

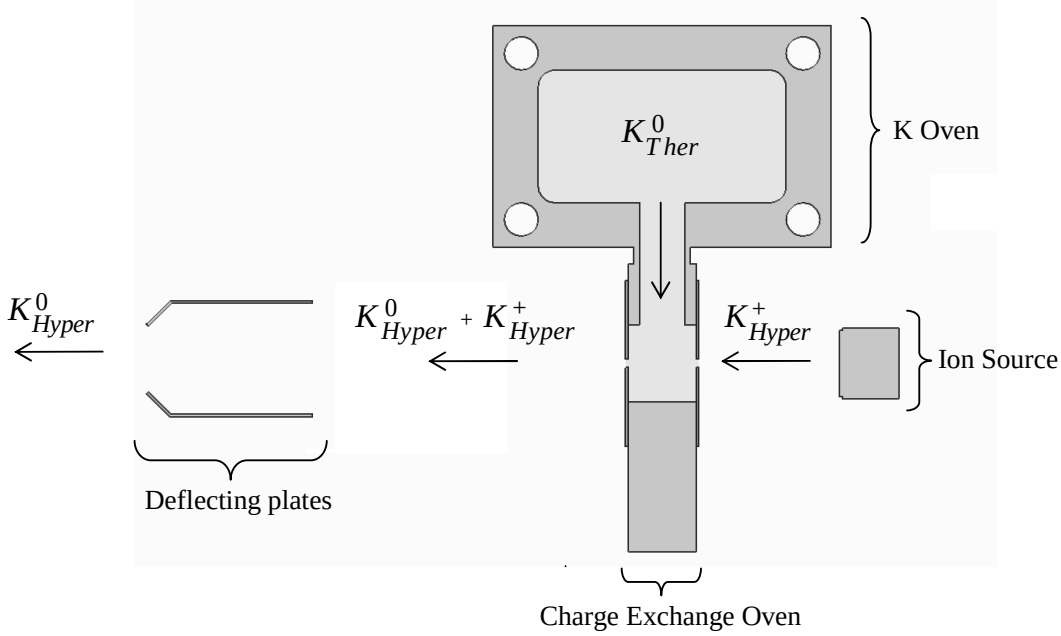

Figure 3.2: Charge exchange system schematics. Taken from [26]

3.1.3 Langmuir-Taylor Surface Detector

The Langmuir-Taylor detector (figure 3.3) is placed at the entrance of the collision chamber in order to monitor the potassium neutral beam that reaches this point. It consists of a stainless steel cylindrical collector placed around a high purity ($> 99\%$) iridium filament. The collector has two holes along the beam axis and the filament is placed above the main section of the beam, in order to minimize interfering with it.

By applying a current to the filament, a cloud of electrons is created in its vicinity with sufficient energy to ionize the neutral hyperthermal potassium atoms that pass through the detector. The generated potassium ions are repelled outwards and detected in the collector as a result of an applied positive voltage to the filament. The collector is connected to an electrometer referenced to ground potential, allowing one to measure the generated ionic current, which is proportional to

the hyperthermal potassium atoms beam intensity. A typical current of 0.63 A is applied to heat the filament, whereas +60 V are applied in order to repel the ionized potassium.

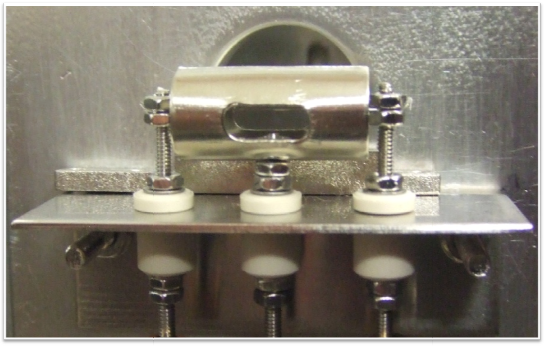

Figure 3.3: Langmuir-Taylor detector.

3.1.4 Molecular Target Oven

The molecular target oven (figure 3.4) is composed of a copper outer body, a removable stainless steel sample holder that fits into the outer body through a back opening, and a copper capillary tip. The outer body is also connected to a liquid and gas sample admission system.

The oven is heated through a halogen bulb and surrounded by a stainless steel reflector to increase the bulb's heating efficiency. The bulb's intensity is controlled by a variac and the outer body temperature is monitored by a K-type thermocouple.

The oven is set on a platform allowing for a fine alignment with the collision center.

3.1.5 Time-of-Flight Mass Spectrometer

3.1.5.1 Working Principle

The time-of-flight mass spectrometer is founded on the simple principle that charged particles with different mass-to-charge ratios (m/z), when subjected to the same force, obtain different velocities and thus will take different flight times along a fixed field-free region.

The most elementary version of a TOF mass spectrometer comprises an extraction region, a field-free drift region and a detector as depicted in figure 3.5. In the extraction region, the ions are accelerated by means of a repulsive voltage applied

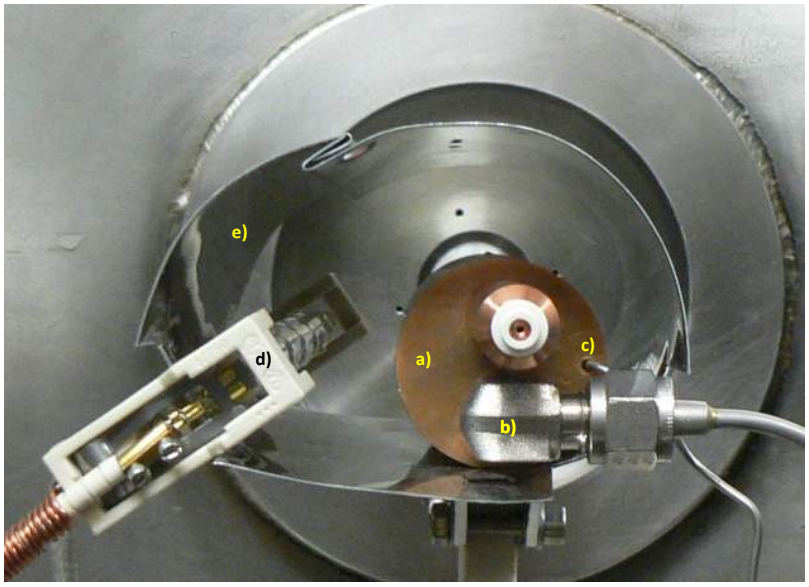

Figure 3.4: Picture of the molecular target oven. a) Molecular target oven - outer body; b) Gas and liquid samples inlet system; c) Thermocouple; d) Heating lamp; e) Radiation deflector. Adapted from [56].

to the extraction plate, setting an electric field between the plate and the drift region. The extracted ions cross the drift region with velocities that are inversely proportional to the square root of their masses. This means that heavier, hence slower, ions will arrive at the detector after the lighter ions with higher velocities.

Depending on the drift region length and the extraction potential applied, ion flight times fall in the range of 10 to 200 μs. Such fact represents a significant advantage of TOF devices in comparison to other types of mass spectrometers, since a complete mass spectrum is obtained within several tens of microseconds.

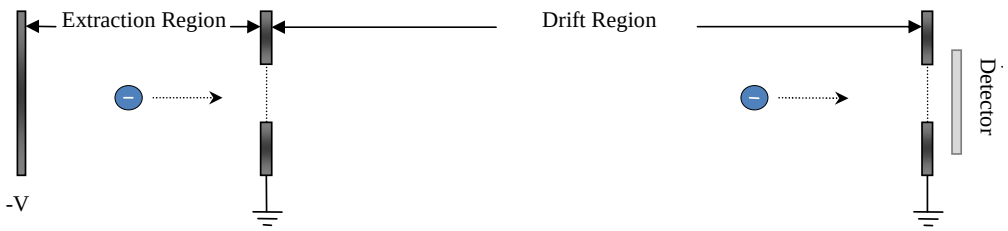

Figure 3.5: Single-stage TOF mass spectrometer schematic. Adapted from[26].

3.1.5.2 Implemented TOF

There have been several improvements to the simple design described above, such as reflectron type TOF spectrometers, with the intent to increase the mass resolution of the spectrometer. Within the scope of the research work carried out in Lisbon, the configuration used is a dual-stage time-of-flight system (Wiley-McLaren geometry [57]). The main upgrade of this geometry from the single-stage one is the introduction of a second extraction region, called acceleration region, that allows longer field-free regions maintaining the possibility to rectify the flight time of ions with the same mass created at different initial positions. Both the flight time and space-focusing are two of the most significant parameters regarding mass resolution.

The TOF mass spectrometer used, pictorially presented in figure 3.6, consists of an extraction region (which corresponds to the collision region), an acceleration region, an einzel lens system, a set of deflecting plates, a field-free drift tube and a channeltron detector.

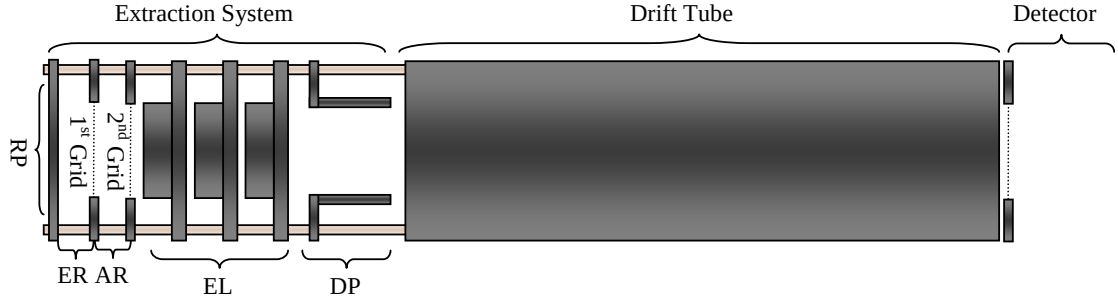

Figure 3.6: Schematic of the implemented TOF mass spectrometer. RP: Repeller plate; ER: Extraction Region; AR: Acceleration region; EL: Einzel lens system; DP: Deflecting plates. Adapted from[26].

Extraction and Acceleration Regions

The extraction region is where the neutral potassium and molecular beam collide. It consists of two electrodes (repeller plate and first grid) 1.2 cm apart. Before reaching the collision region both beams are made to pass collimating slits to avoid saturation.

Upon electron transfer from neutral potassium atoms to the molecular target and consequent formation of anionic molecular fragments, the latter are extracted by means of a fast rise (usually 1.25μs) pulsed voltage signal applied to the lower

repeller plate consisting of a -350 V pulse added to a -3500 V constant value, causing the negative ions to leave this region into the acceleration region.

Ions entering this region suffer a significant acceleration due to the -3500 V constantly applied to the first grid with respect to the second grid referenced to the ground, causing them to enter the einzel lens region and ultimately the drift region and detector. When the -350 V pulse is active, the particles will leave the extraction system with a total energy of 3850 eV. Whereas when the pulse is not active, the voltage difference between the repeller plate and the first grid is zero, and the particles are not extracted. Thus, this pulsed signal is used as a start signal for the time-of-flight measurements.

Einzel Lens System

The purpose of the einzel lens system is to concentrate and converge the ions extracted from the collision region to the channeltron detector, optimizing the detection and the yielded signal. This set works like an optical lens system, forcing the ions to converge to a focal point without changing its energy. It comprises three aligned cylinders, where a voltage is applied to the central one and the others are grounded. Several tests upon the apparatus assembling allowed to conclude that the optimal voltage to apply is -1500 V. With the same purpose, a set of deflecting plates were also assembled after the einzel lens system. However, the deflecting plates are grounded since they were found to be irrelevant to the signal improvement.

The voltages applied to the extraction system are summarized in figure 3.7.

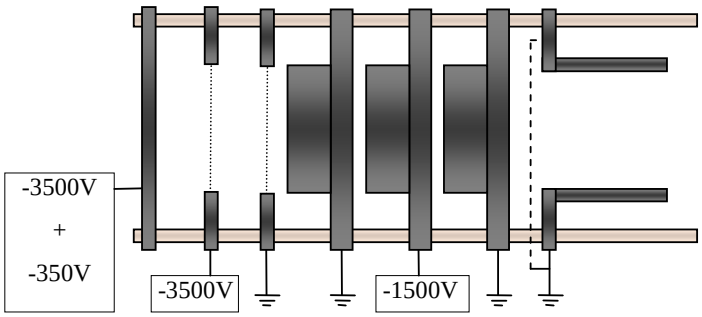

Figure 3.7: Voltages applied to TOF extraction system. Adapted from[26].

Channeltron Detector

The channeltron detector is a device that from the impact of charged particles

emits secondary electrons. Due to a voltage drop of about 2000 V between the entrance and the rear end of the detector, the electrons collide once again with the channeltron's walls, generating a cascade of electrons. As such, for each ion impact, the detector generates a negative voltage pulse with 20 ns duration and an amplitude of typically -20 mV.

TOF Mass Spectra

Once in the field-free region, ions with different masses will reach the detector at different time intervals. Since the time of flight is proportional to the square root of (m/z) and that all fragments have the same charge (-e), the resulting spectrum assigns to every channel a given mass. Each channel corresponds to a 8 ns time window. The time-of-flight starts from the moment the extraction pulse is applied.

3.1.6 Vacuum System

The vacuum system comprises two chambers (potassium chamber and collision chamber) differentially pumped.

The vacuum conditions in the potassium chamber are guaranteed by a diffusion pump and a liquid nitrogen trap to avoid migrations of diffusion pump oil into the chamber. The diffusion pump backup is guaranteed by a two-stage rotatory pump with a magnetic valve and a sieve trap in between to prevent the contamination with rotatory oil vapours.

The vacuum conditions in the collision chamber chamber are guaranteed in a similar way as the one described in the potassium chamber case. The high-vacuum is achieved by a diffusion pump. The TOF system is pumped differentially by a turbomolecular pump placed near the channeltron detector. Both the turbo and the diffusion pumps are backed up by a two-stage rotatory pump. The liquid and gas sample inlet system is also differentially pumped by a two-stage rotatory pump.

Both chambers are connected through a manual gate valve that allows an independent chamber operation. Therefore, it is possible to operate one of them at atmospheric pressures keeping the other in high-vacuum conditions, which is important when cleaning the collision chamber or potassium replacement is needed.

The rotatory pumps provide an ultimate pressure of 1 Pa. Only after primary vacuum pressures are reached the pumping is changed to the diffusion and turbomolecular pumps, which provide high-vacuum pressures, in the order of 10^{-5} Pa. The pressures are monitored by pirani type units for primary vacuum and penning type units for high-vacuum.

It is relevant to stress the importance of achieving vacuum in the conditions described, since it is related to mean free path, i.e. the average distance that a particle travels between collisions. The mean free path is given by:

$$\lambda \cong \frac{7 \times 10^{-3}}{WorkingPressure}(cm) \tag{3.2}$$

Considering that during measurements the base pressure is around 6×10^{-5} Pa, the mean free path is approximately 116 m. Given that the distance between the plane where the potassium ions are generated and the collision region is about 50 cm, it is fair to state that the measurements are performed under single-collision conditions.

3.2 Dissociative Electron Attachment Experimental Set-up

3.2.1 Apparatus Overview

Free electrons are made to collide with a molecular target by means of a crossed beam arrangement as shown in figure 3.8, where negative ions resulting from dissociative electron attachment are detected.

The apparatus consists of one high-vacuum chamber. An electron beam with well-defined energy is generated by a trochoidal electron monochromator (TEM) and focused into the reaction region. Two halogen bulbs heat the chamber with two purposes: (1) to sublimate the solid samples generating an effusive molecular target beam, and (2) to prevent condensation of the sample in the lens system and walls of the chamber. The temperature inside the chamber is controlled by a PT100 resistor. The sublimated molecular beam is guided through a capillary towards the collision region. Negative ions formed from the electron-molecule collision are mass analysed by a quadrupole mass spectrometer (QMS) and detected by a secondary electron multiplier (SEM).

In order to have a resonance spectrum of a specific anionic fragment, the mass spectrometer is fixed to a constant mass and the ion yield is recorded as function of the incident electron energy. Although the opposite measurement is also possible, i.e. setting the electron energy to a fixed value one can obtain a mass spectrum of the formed negative ions. The TEM, and therefore the electron energy, is controlled by the computer.

Gas and liquid samples with high vapour pressure are admitted into the chamber through a gas-inlet system (Swagelok) with a leak valve incorporated. The system is also equipped with a SF_6 gas cylinder, allowing for energy calibration with the known resonance spectrum for this compound, as described in subsection 3.2.4. Further details can be found elsewhere [9, 58]

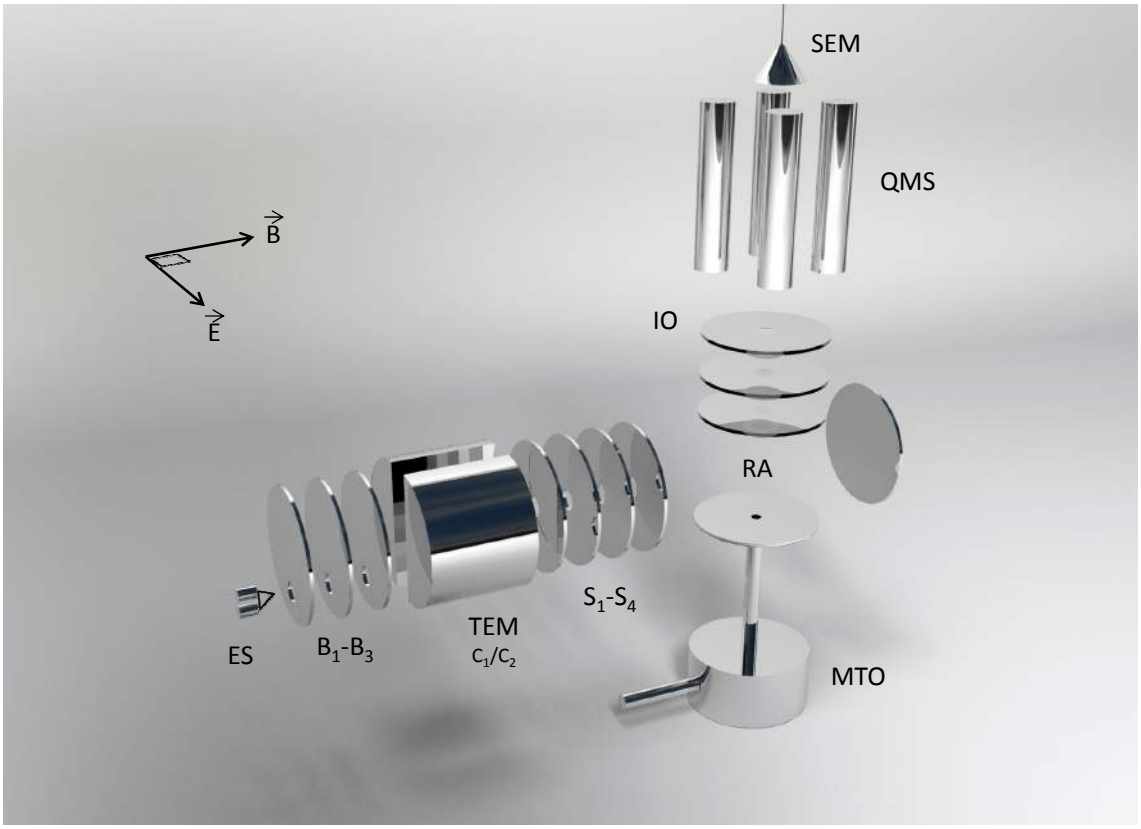

Figure 3.8: Schematic of the dissociative electron attachment experimental device. ES: Electron source, $B_1 - B_3$: Focusing lenses with non-axial holes, TEM: Trochoidal electron monochromator, $S_1 - S_4$: Focusing lenses with axial holes, RA: Reaction area, MTO: Molecular target oven, IO: ion optics, QMS: Quadrupole mass spectrometer, SEM: Secondary electron multiplier, $\overrightarrow{E}$: Electric field (y-direction), $\overrightarrow{B}$: Magnetic field (x-direction).

3.2.2 Monoenergetic Electron Beam

The electrons are emitted from a hot tungsten filament supplied with a current of approximately 2.3 A. A set of three electrodes with non-axial holes following the filament (B_1-B_3) focuses the electrons into the deflection region, where the energy selection takes place.

A TEM is placed with the purpose of generating a monoenergetic electron beam from the beam with high energy distribution emitted from the filament. The trochoidal electron monochromator (deflection region) consists of two parallel flat lenses that generate an homogeneous electric field (y-direction) by applying a potential difference between the plates. An axial magnetic field (x-direction) is generated externally by two Helmoltz coils. Thus the electrons find themselves in a crossed electric and magnetic fields in the deflection region, describing trochoidal trajectories with its guiding center moving in the z-direction, with a constant velocity that depends on the ratio between the strengths of the electric and magnetic fields [59]:

$$v_z = \frac{|\vec{E} \times \vec{B}|}{B^2} = \frac{E}{B} \tag{3.3}$$

Where E and B are the electric and magnetic fields, respectively. The electrons with different kinetic energies, thus different velocities, entering the monochromator spend different times in the crossed field region and therefore dispersion occurs along the z-direction as a function of the initial axial velocity. The next lens (S_1) possesses an axial hole, displaced by some distance with respect to the entrance aperture (B_1-B_3). As such, only the electrons having a certain velocity and thus a corresponding deflection in the z-direction reach the exit aperture and are transmitted in the new axis. The dispersion effect in the deflection region is shown in figure 3.9.

The set of lenses S_1-S_4 refocusses and accelerates or decelerates these energy selected electrons into the reaction zone, where they interact with the effusive molecular beam. After passing through the reaction zone, the transmitted electrons are collected by one lens which serves as a beam intensity monitor. The measured current is usually 10-20 nA. During measurements the resolution of the electron beam can be controlled by changing the potential difference between C_1 and C_2 and hence the electric field E, whereas the beam intensity may be optimized by changing the voltages applied to the electrodes (lens) system.

The apparatus configuration described is known to be suited to the study of electron attachment reactions [9]: (1) the axial magnetic field prevents spreading of the electron beam at low energies, which may be useful when performing experiments with electrons with near 0 eV; (2) the magnetic field aligns the electron beam, allowing an effective separation of electrons and negative ions at the detector.

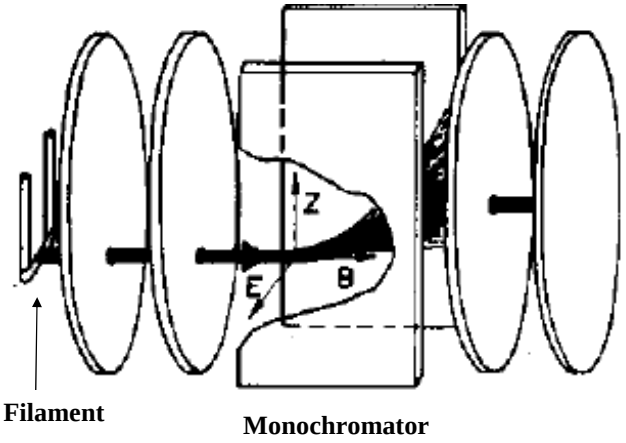

Figure 3.9: Trochoidal electron monochromator arrangement: dispersion effect. Adapted from [59].

3.2.3 Ion Extraction and Detection

Ions formed in the reaction zone from the interaction between the electron beam and the target gas beam are extracted by a weak electric field (in the order of 1 V/cm) in the z-direction into the quadrupole mass filter. Before reaching the QMS, the ions are refocused by a series of parallel electrodes called ion optics.

A QMS consists of four rods where a voltage comprising a constant component (U) and a radio-frequency component ($V \cos \omega t$) is applied, creating a two-dimensional alternating quadrupole field between them. Opposite rods are electrically connected pairwise. A schematic of the QMS arrangement is shown in figure 3.10. A given U/V ratio corresponds to a single mass to charge ratio that allows for a stable trajectory along the QMS path, that is only ions with a specific mass to charge ratio are transmitted trough the quadrupole of finite length. The other ions strike the rods and get neutralised. Hence, ions can be selected according to *m/z* by setting the direct and alternating voltages ratio.

The mass-selected negative ions are collected by a secondary electron multiplier. The SEM consists of 17-stage CuBe dynodes supplied with a 3.4 kV voltage. Ions hitting the detector generate secondary electrons which, in turn, are accelerated towards the next dynode and so on, generating an electron pulse at the collector. The final pulse is decoupled, amplified, read by the computer and displayed as ion count rate.

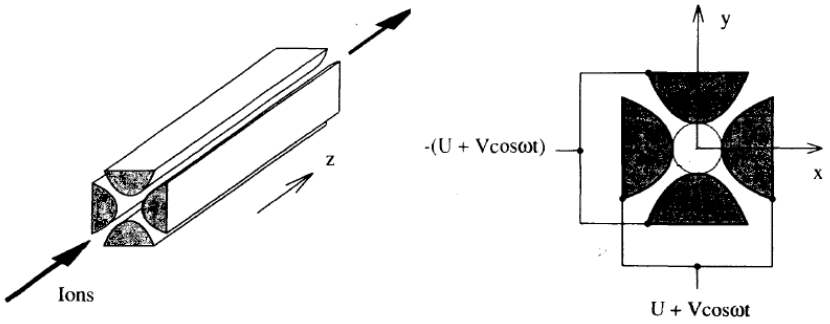

Figure 3.10: Quadrupole mass spectrometer arrangement. Adapted from[9].

3.2.4 Energy Scale Calibration

The energy scale of the obtained spectra is calibrated by measuring dissociative electron attachment to SF_6, which generates a known sharp peak resonance associated with the formation of metastable SF_6^- very close to 0 eV electron energy. The width of the resonance is known to be below 1 meV [60]. The full-width at half maximum (FWHM) of the SF_6^- resonance in the conducted experiments is only limited by the resolution of the electron beam upon interaction. Hence, the FWHM is used to determine the electron energy resolution.

3.2.5 Vacuum system

The set-up components are housed in a high-vacuum chamber that is pumped by a turbomolecular pump capable of achieving a base pressure of 10^{-5} Pa, supported by a rotatory vane pump that provides an ultimate pressure in the order of 10^{-1} Pa. The gas and liquid samples inlet tubes are also pumped by a rotatory vane pump and can be heated with a heating band.

Chapter 4

Results and Discussion

The aim of the present work is to study the fragmentation pattern of sulphur containing biological relevant molecules through dissociative electron attachment and electron transfer upon potassium-molecule collisions, and ultimately try to better understand the role of the sulphur atom in such reactions.

On the first section of this chapter the experimental conditions for both studies are summarized. On the following sections the results of electron driven reactions to thiaproline and taurine are presented and discussed with a comparative analysis of both dissociative mechanisms.

4.1 Experimental Conditions

4.1.1 Dissociative Electron Attachment Measurements

The experimental results of dissociative electron attachment to thiaproline and taurine were obtained in a crossed-beam set-up described in section 3.2.

The anionic fragments arising from the interaction of free electrons with the target molecules were detected and its intensity recorded as a function of the incident electron energy. Mass scans were also obtained, where the intensity of the yielded fragments for a fixed incident electron energy was recorded as a function of its mass.

The thiaproline and taurine samples were obtained from Sigma Aldrich with a stated purity of 98% for thiaproline and $\geq$ 99% for taurine, and used as delivered. An effusive molecular beam is generated from solid samples by heating the container. The optimum temperature is controlled by the ion signal intensity and the measured chamber pressure. In the present case, such temperature was found to be 412 K for thiaproline measurements and approximately 438 K for

taurine. It should be noted that a possible thermal decomposition of the molecules was considered. However, this can be excluded for two reasons: (a) no noticeable change in the ion intensity ratios was observed when the temperature was further increased, as it would be expected for thermal decomposition, and (b) nuclear magnetic resonance (NMR) spectra of the original and heated samples did not reveal any differences between them.

The work pressure was 4×10^{-5} Pa and 8×10^{-5} Pa for thiaproline and taurine measurements, respectively. The base pressure was 3×10^{-6} Pa. The spectra acquisition parameters, such as the number of bins, the energy range and the dwell time, were kept constant throughout the experiments: a total of 800 bins corresponding to a 12 eV range were used and the ion count signal was recorded during 1 second for each energy bin.

The raw resonance intensity is plotted as a function of the bin number and thus need to be energy calibrated. To do so, a sharp peak resonance associated with the formation of metastable SF_6^- very close to 0 eV electron energy is used, as described in section 3.2.4. The bin corresponding to the maximum value of the peak corresponds to 0 eV energy. From that and from the total number of bins-energy range correspondence is possible to derive an energy calibration equation.

SF_6 gas is introduced in the chamber before and after completing the molecular target measurements not only for energy calibration, but also to allow for the improvement of the energy resolution of the apparatus. The resolution is controlled by the FWHM of the 0 eV SF_6^- resonance and its improvement is achieved by changing the voltage values applied to the several electrostatic lens (see section 3.2), as well as the potential difference between the two plates of the trochoidal electron monochromator. The achieved energy resolution in the performed measurements was approximately 150 meV.

4.1.2 Electron Transfer Measurements

The experimental results of electron transfer in atom-molecule collisions were obtained in a crossed-beam set-up described in section 3.1. The molecular targets' negative ion formation arising from the collision with neutral potassium atoms was probed at different collision energies defined within a laboratory framework: thiaproline was made to collide with neutral potassium atoms with kinetic energies of 12, 17, 30, 50, 70 and 100 eV, and taurine measurements were performed for collision energies of 30, 70 and 100 eV.

As described in section 2.2.3, the available energy for electron transfer to occur is equivalent to the collision energy in the centre-of-mass framework and is obtained from equation 2.16. This approximation can be made assuming that the target molecule is motionless, i.e. that the velocity of the molecule (which is at a thermal energy) is negligible in comparison to the velocity of the potassium atom. Table 4.1 summarizes the available energies for both molecular targets and for the different acceleration voltages.

Table 4.1: Available energies in the centre-of-mass framework.

	$E_a(eV)$	
$E_{lab}(eV)$	Thiaproline	Taurine
12	3.92	3.80
17	7.36	7.19
30	16.30	16.00
50	30.06	29.57
70	43.82	43.13
100	64.46	63.47

The negative ions resulting from the collision were extracted by a -350 V/cm pulsed electrostatic field with a 1.25μs duration, consistent for all measurements.

The molecule samples were obtained from Sigma Aldrich with the same purity mentioned above, and used as delivered. Since both were solid samples, it was necessary to heat them in order to generate an effusive beam towards the collision region. During measurements thiaproline was heated to a temperature of about 385 K, while for taurine the density of intact molecules was high enough to yield a good signal at a temperature of about 485 K. The temperature necessary to vaporize the samples must be thoroughly controlled to avoid thermal decomposition of the molecules. No noticeable change in the ion intensity ratios was observed when the temperature was further increased, which allows one to conclude that the molecules did not suffer thermal decomposition and thus reached the collision region intact.

Despite being similar, the heating temperatures used in DEA and electron transfer experiments were found to be different. Such difference accounts for the much different heating system and dynamics for both apparatus, as described in chapter 3. While on the electron transfer set-up the heating temperature is achieved by means of three halogen bulbs in the chamber and one placed near the molecular target oven, in the DEA set-up a much smaller chamber is heated by two halogen bulbs, sufficient to generate the effusive molecular beam.

The hyperthermal neutral potassium beam's intensity was measured in the Langmuir-Taylor detector (section 3.1.3) before and after each spectrum acquisition. The same was done to monitor the ionic current in the deflecting plates (section 3.1.2).

The time-of-flight acquisition parameters, such as the number of bins and the bin width, were kept constant throughout the measurements: a total of 4096 bins with 8 ns width were used. Tables 4.2 and 4.3 summarize the experimental parameters registered in the collection of spectra for thiaproline and taurine, respectively.

Table 4.2: Experimental acquisition parameters registered for potassium-thiaproline collisions.

	12 eV	**17 eV**	**30 eV**	**50 eV**	**70 eV**	**100 eV**
Acquisition time (s)	102600	94400	74800	8000	4000	6000
Langmuir-Taylor current (mean value) (pA)	0.89	0.58	0.29	3.80	21.39	65.38
Deflecting plates current (mean value) (nA)	0.62	0.90	7.86	21.06	37.94	66.55
Collision chamber work pressure (Pa)	—— 2×10^{-4} ——					
Collision chamber base pressure (Pa)	—— 7×10^{-5} ——					

Table 4.3: Experimental acquisition parameters registered for potassium-taurine collisions.

	30 eV	**70 eV**	**100 eV**
Acquisition time (s)	77000	15000	10800
Langmuir-Taylor current (mean value) (pA)	1.09	2.61	17.12
Deflecting plates current (mean value) (nA)	3.95	17.29	24.42
Collision chamber work pressure (Pa)	—— 1×10^{-4} ——		
Collision chamber base pressure (Pa)	—— 7×10^{-5} ——		

In addition to the spectra acquired with the temperatures mentioned above, spectra of the residual gases, designated by background spectra, were also acquired for the same energies in order to subtract the latter to the first. For the subtraction

to be valid the spectra must be normalized according to the following expression:

$$\frac{C}{t \times I_{LT}} \tag{4.1}$$

Where C is defined as the ion count per channel, t is the acquisition time and I_{LT} is the mean value of the neutral potassium beam intensity, measured in the Langmuir-Taylor detector. Furthermore, such normalization allows to compare between spectra acquired at different collision energies.

After subtracting the background a smoothing type filter was applied. The baseline of the spectra was subtracted with the purpose of removing the background noise. Moreover, some peaks in the mass spectra appeared with a shoulder to the right (especially the low masses), due to the contribution of the ions created during the extraction process, which was removed upon baseline subtraction.

Before and after the aforementioned treatment, the spectra were individually calibrated, each channel corresponding to a respective mass. The calibration was achieved making use of known and easily identifiable peaks of the molecule spectra and of nitromethane spectra acquired after the target molecule measurements. Nitromethane mass spectra have already been extensively studied and well characterized. The remaining peaks (fragments) were identified by fitting a parabolic curve (characteristic of time of flight spectrometry) to the correspondence between channel and mass for the known peaks.

4.2 Taurine

Taurine's (T) chemical structure ($C_2H_7NO_3S$) is depicted in figure 4.1. Its composition gives a total molecular weight of 125.5 g/mol (125 a.m.u.).

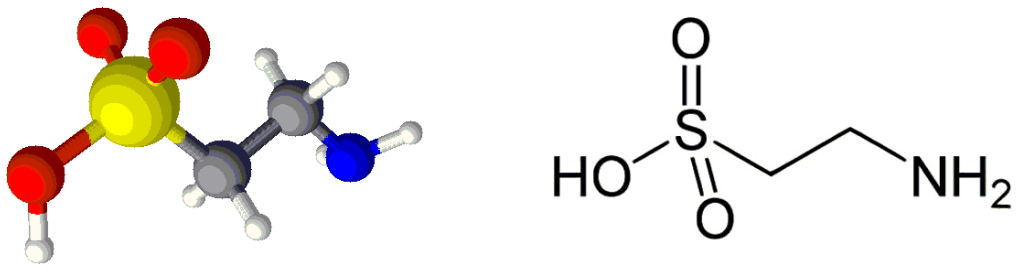

Figure 4.1: Schematic representation of taurine molecule: three-dimensional (left) and two-dimensional (right) models. White - hydrogen, black - carbon, blue - nitrogen, red - oxygen, yellow - sulphur.

4.2.1 Dissociative Electron Attachment Results

The impact of low energy (<12 eV) electrons on taurine leads to the formation of four anionic fragments at mass to charge ratios (*m/z*) 124, 46, 16 and 1. Two of them, namely 124 and 1 a.m.u. that have been ascribed to $[T-H]^-$ (i.e. the dehydrogenated parent molecule) and H^- anions, arise from a direct single bond rupture. The assignment of the fragment ions at 46 and 16 a.m.u. to a stoichiometric composition is ambiguous. In fact, the first may be ascribed to either CH_2S^-, NS^- or NO_2^- ions, while the latter can be NH_2^-, O^- or a combination of both.

The change in the ion intensity with respect to the incident electron energy represent structures reminiscent of resonant mechanisms for the ion production. The ion yield functions are displayed in figures 4.2 and 4.3. Table 4.4 reports the peak positions (maximum intensity) obtained from gaussian peak fittings of the observed resonances.

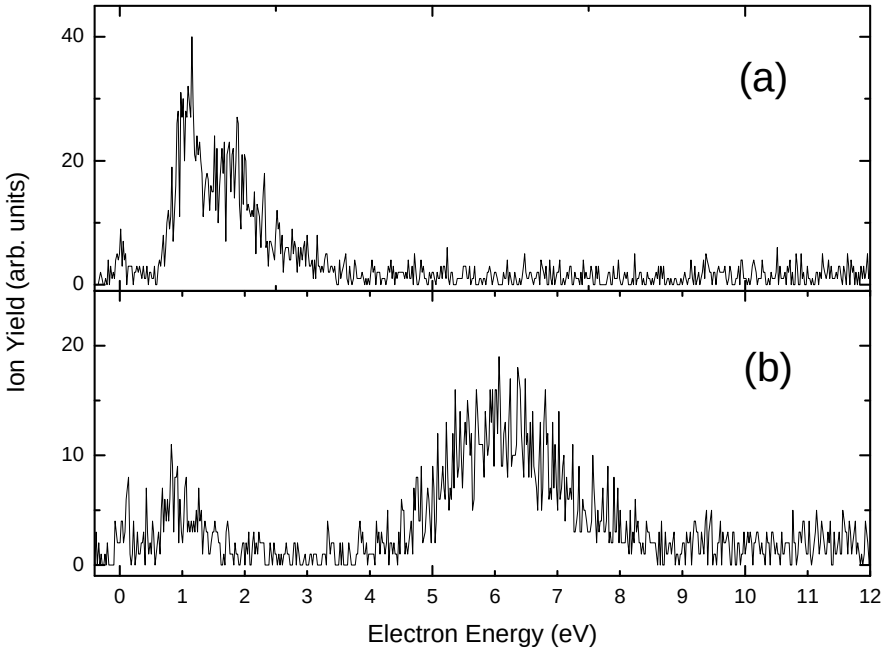

Figure 4.2: Ion yield of (a) $[T-H]^-$ (*m/z* 124) and (b) H^- (*m/z* 1) as a function of the incident electron energy.

The dissociation process induced by electron attachment also generates neutral (radical) fragments. However, its composition is not directly accessible from the present experiment.

The most dominant fragment anion was observed at 46 a.m.u. within a narrow peak at threshold (~0 eV). The production of either of the assigned possible fragments (CH_2S^-, NS^- and NO_2^-) requires substantial rearrangement associated

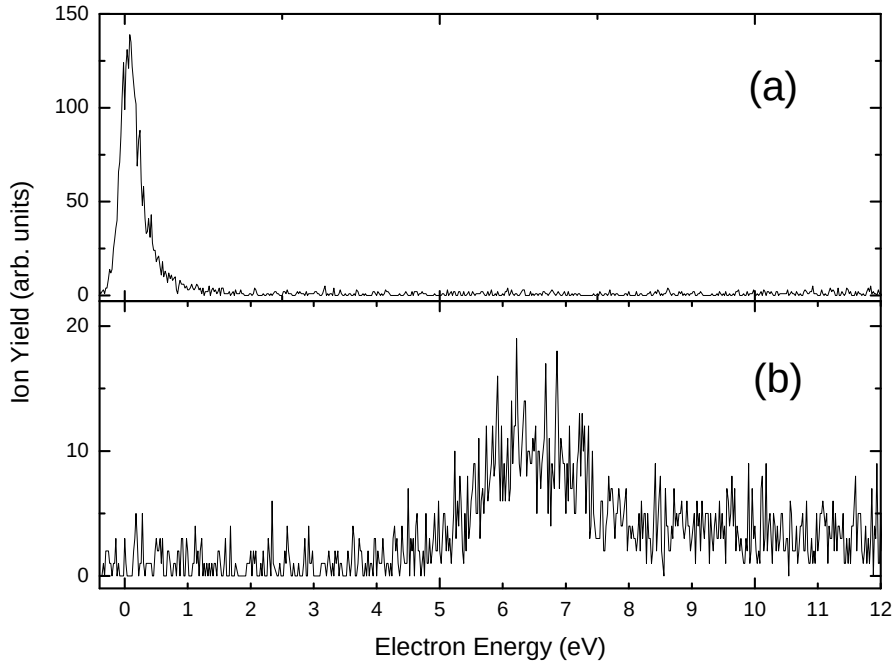

Figure 4.3: Ion yield of (a) *m/z* 46 and (b) *m/z* 16 as a function of the incident electron energy.

Table 4.4: Resonance positions of the anionic fragments generated from DEA to taurine.

Ion	*m/z*	Electron energy (eV)		
$[T-H]^-$	124	0	1.1	1.7
CH_2S^- / NS^- / NO_2^-	46	0.1		
NH_2^- / O^-	16			6.5
H^-	1		0.9	6.1

with multiple bond cleavage. Hence, the overall reaction can only proceed through a concerted process forming new bonds to supply the necessary energy. This could be in part possible due to the relatively high electron affinity of these radical anions, specially NS^- and NO_2^- (1.19 eV and 2.27 eV, respectively [61]).

The appearance energy (AE) of the negatively charged species can be estimated as the difference between the bond dissociation energy (BDE) and the electron affinity (EA) of the fragment where the excess charge is localised (cf. equation 2.5). However, this estimation is valid only for a simple bond dissociation. For a more complex fragmentation scheme or when additional vibrational energies have to be considered, the AE value may change.

As mentioned above, the 16 a.m.u. feature may comprise contributions from NH_2^- and/or O^-. Energy arguments suggest the formation of O^- rather than

NH_2^-, since the electron affinity of O (1.46 eV) is almost twice that of NH_2 (0.77 eV) [61]. However, it would not be reasonable to completely rule out the contribution of NH_2^- to the ion yield.

The O^- can result from cleavage of the S=O double bond (reaction A) or from a concerted reaction where the oxygen atom is removed from the hydroxyl group (OH) and the hydrogen atom from the same group is transferred to the parent molecule (reaction B), as represented in figure 4.4. The radical anion NH_2^- arises from the cleavage of a single C−N bond (reaction C, figure 4.4). From the electron affinity (EA) of the oxygen atom and the S=O bond dissociation energy (4.86 eV [62]) it is possible to derive the thermodynamic threshold for reaction A: 3.4 eV. The appearance energy for reaction C is estimated to be 2.91 eV, considering the dissociation energy for the $C_2H_5 - NH_2$ bond of the ethylamine molecule (3.68 eV [63]). As can be seen from figure 4.3, the appearance energy (i.e. the left-hand side peak threshold) amounts to 4.5 eV and thus lies above the calculated appearance energies for both fragments. Hence, one must consider the contribution of both anions for the broad resonance found at 16 a.m.u..

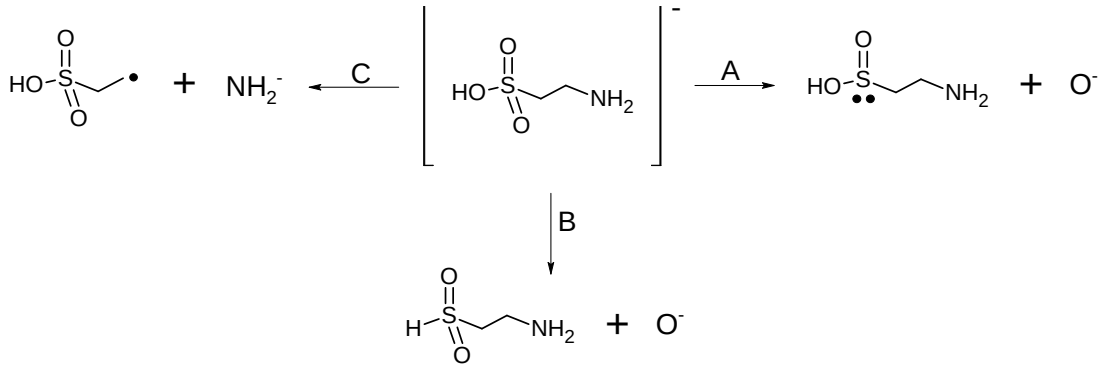

Figure 4.4: Possible dissociation pathways for (A and B) O^- and (C) NH_2^- production after low-energy electron attachment to taurine.

The three mentioned mechanisms for 16 a.m.u. ion production have been also discussed in DEA to cysteine (a sulphur containing amino acid similar to taurine, with a COOH group instead of SO_3H) [64]. In fact, the reported resonance profile for such ion is similar to the one presented in this work in terms of peak position and onset for the ion formation. However, in their case, the calculated dissociation energy for the $C - NH_2$ bound leads to an appearance energy of 6.0 eV, which is above the experimentally observed AE. From that, the formation of NH_2^- was ruled out. However, the authors probably used the dissociation energy for a simple C-N bond in their calculations, when in fact the reaction implies the dissociation of an amino group (NH_2) from a carbon chain. Hence, the dissociation energy for

the $C_2H_5 - NH_2$ bond of the ethylamine molecule is believed to be more accurate. DEA to glycine results [65] show two peaks for 16 a.m.u. ion, where the low energy resonance is unambiguously attributed to NH_2^- and the other to O^-, thus corroborating the presented analysis.

It is noteworthy that the contribution from reaction C should not be excluded. It has been reported that taurine is dominated by a single conformer that is stabilized by an intramolecular O−H···N hydrogen bond established between the amino and sulfonic groups, as depicted in figure 4.5 [66]. This stable conformer may facilitate the single S-OH bond cleavage, yielding the anion O^- and the neutral fragment $[T - O]$.

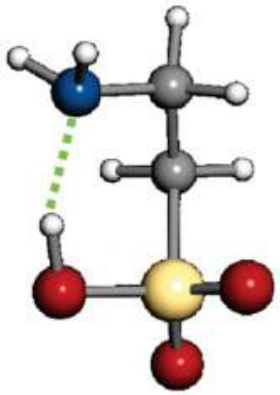

Figure 4.5: Schematic representation of the stable conformer of taurine molecule: intramolecular hydrogen bond is represented by the green dashed line. Adapted from [66].

In contrast to the complex reactions involving multiple bond cleavage to form the anion at 46 a.m.u., the other detected fragments may result from simple bond cleavage leaving the rest of the taurine molecule unchanged.

The fragment H^- is formed within two resonances near 1 and 6 eV. The estimate for the thermodynamic thresholds for the loss of H from the oxygen, nitrogen and carbon positions is 3.70, 2.76 and 2.75 eV respectively, considering the EA of H (0.75 eV) and the respective bond dissociation energies (4.46, 3.51 and 3.50 eV [61]). For this reason, the most intense resonance found at 6.1 eV may arise from the three dissociative channels. However, given the higher electronegativity of the oxygen atom, H^- is more likely to arise from the hydroxyl group. The resonance at 0.9 eV lies below the calculated appearance energies and therefore such reaction proceeds through molecular rearrangement and formation of new bonds or new stable molecules to supply the necessary energy for it to occur.

The loss of an hydrogen atom may yield two complementary anionic fragments (H^- and $[T-H]^-$), depending where the extra negative charge is localised. The dehydrogenated parent anion is more dominant than the first and exhibits three resonant dissociation channels. The resonances found for both fragments at 0.9 and 1.1 eV may result from the same reaction channels. Although it is not undoubtedly clear from the presented H^- spectra, there seams to be a peak at 0 eV electron energy that may be associated with that for $[T-H]^-$. Better signal-to-noise ratio and resolution would be required to confirm.

At energies above approximately 3-4 eV, the capture of the incoming electron most likely proceeds from core excited resonances (2 particles - 1 hole), where electronic excitation of the molecule is possible. That is the case of the lighter observed fragments NH_2^- / O^- and H^-. Resonances appearing at energies below 4 eV, as is the case for the heavier anionic fragments at 46 a.m.u. and $[T-H]^-$, may be explained by a initial formation of a vibrational Feshbach resonance, which can be supported by the very large dipole moment of taurine (15.5 D [67]). The electron gets trapped in a very diffuse Rydberg-like orbital, forming a dipole-bound state. Such state can couple to a valence state, which then leads to dissociation. Still, it is remarkable that electrons below 0.5 eV are able to induce this manifold bond-breaking reactions, specially the one generating the fragment with *m/z* 46.

4.2.2 Electron Transfer Results

The TOF mass spectra obtained for potassim-taurine collisions at 30, 70 and 100 eV are presented in figure 4.6. Thirteen different anionic fragments were identified and labelled from A to M. For comparison purposes, a list of the obtained fragments in DEA and electron transfer experiments is shown in table 4.5. The relative cross section (branching ratio) of the fragments was calculated by integrating the mass spectrum at each collision energy.

The results of DEA to taurine are quite contrasting with that for electron transfer in terms of number and composition of the resulting negative ions. While thirteen fragments were detected in electron transfer, four were evidenced in free electron attachment. Two negative ions were common to both studies: NH_2^-/O^- (16 a.m.u.) and H^- (1 a.m.u.). The disparity in the results suggests that the mechanism of electron transfer may promote further dissociation of the molecule, most likely due to the presence of the positive potassium core after electron transfer, which suppresses autodetachment of the extra electron from the TNI.

The lowest collision energy, corresponding to 16 eV available energy, is above the resonances measured in DEA. This means that, from an energetic point of

view, NH_2^-/O^- and H^- are equally accessible at 30, 70 and 100 eV. Nonetheless, different relative cross section values are observed for each collision energy. This means that the access to a dissociative channel is not only dependent on the available energy, but also on the effect that the collision energy has in the collision time scale. Indeed, it has been shown that for low collision energies, thus long collision time, if the electron transfer occurs at the first crossing, the coulombic interaction between the formed ions may lead to bond stretching, which increases the probability of ion-pair formation [68]. At higher collision velocities there is not enough collision time for bond stretching and autodetachment becomes dominant. This behaviour is coherent with the decrease of the relative cross section of NO_2^- formation with increasing collision energy in electron transfer to nitromethane studies [21].

Table 4.5: Assigned anionic fragments in DEA and electron transfer to taurine.

		Electron transfer			
Anionic Fragments	*m/z*	30 eV	70 eV	100 eV	DEA
H^-	1	A	A	A	✓
C^-	12	B	B	B	-
CH^-	13	C	C	C	-
CH_2^-	14	D	D	D	-
O^-/NH_2^-	16	E	E	E	✓
OH^-	17	F	F	F	-
C_2^-	24	G	G	G	-
C_2H^-	25	H	H	H	-
$C_2H_2^-/CN^-$	26	I	I	I	-
$C_2H_3^-/CNH^-$	27	-	J	J	-
CH_2CN^-/C_2O-	40	K	K	K	-
$NCO^-/CH_2CO^-/C_2H_4N^-$	42	L	L	L	-
$CH_2S^-/NS^-/NO_2^-$	46	-	-	-	✓
$[T-N]^-/[T-CH_2]^-$	111	M	M	M	-
$[T-H]^-$	124	-	-	-	✓

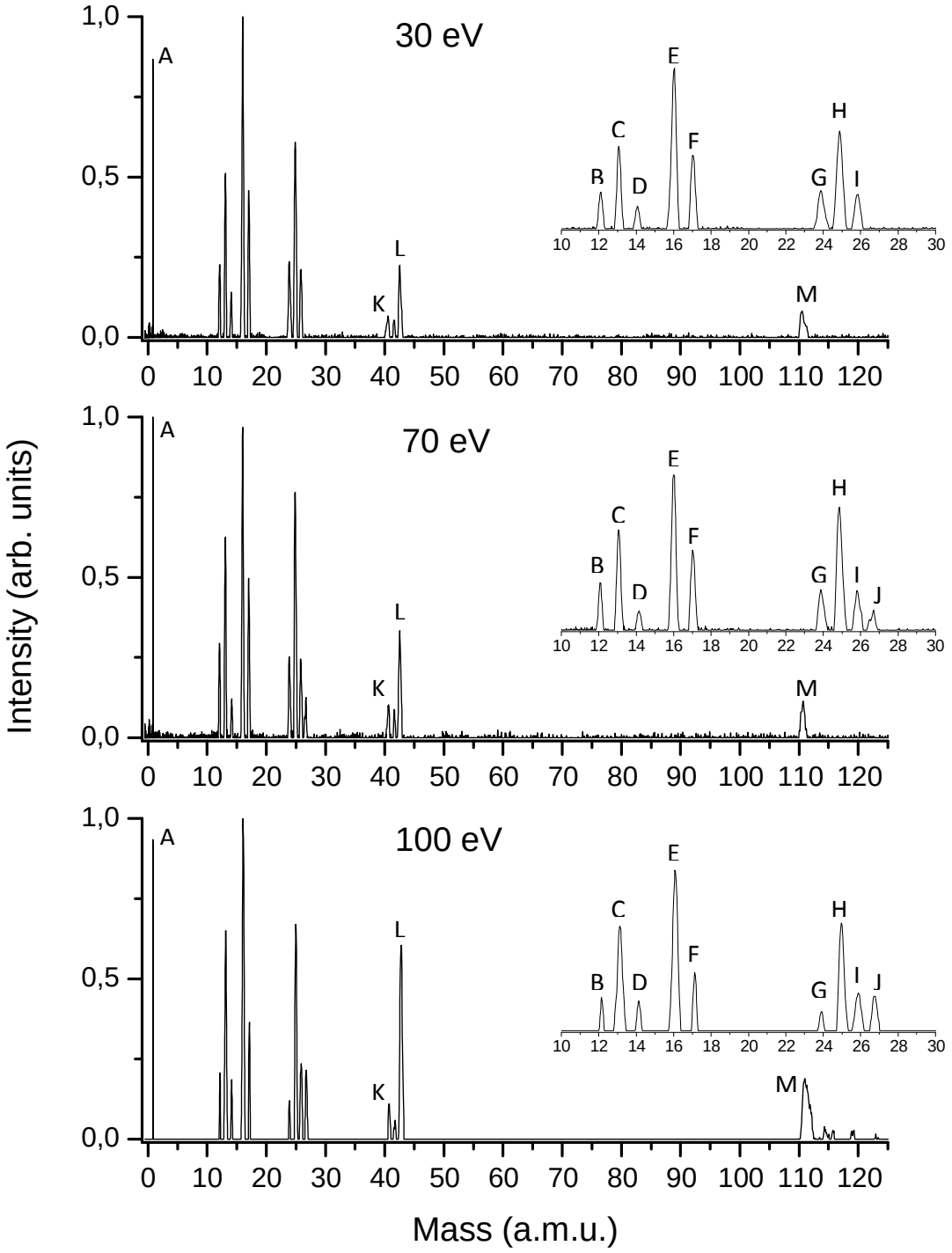

Figure 4.6: Taurine TOF anion spectra at 30, 70 and 100 eV collision energies.

C^- (12 a.m.u.), CH^- (13 a.m.u.) and CH_2^- (14 a.m.u.)

The fragments found at *m/z* 12, 13 and 14 are prominent peaks for the three collision energies, specially the negative ion CH^-. The three must arise from the carbon chain of the molecule, consequently its formation involves cleavage of multiple bonds. The rupture of C-N, C-C or C-S bond generates CH_2^-, which may then loose one or two hydrogen atoms to form the CH^- and C^-, respectively.

The electron affinities of *C* and *CH* (1.26 and 1.24 eV, respectively) are considerably high and almost twice that of CH_2 (0.65 eV [44]). This may explain the higher relative cross section for the first two ions in comparison to the latter. However, the CH^- yield is higher than C^-, which suggests than the the first is somehow stabilized and does not proceed through the loss of the hydrogen atom.

These anions have been also reported in electron transfer studies in potassium-glycine collisions [69] and also for the amino acids alanine and valine [44], whereas in free electron attachment to the referred molecules were not observed.

From a biological perspective, the molecule dissociation through these channels means not only the loss of functionality from taurine molecule but also the possibility of generating H radicals, known for its damaging capabilities.

O^-/NH_2^- (16 a.m.u.)

Fragment anions at 16 a.m.u. represent the most prominent feature in all acquired TOF mass spectra and can be attributed to the isobaric species O^- and NH_2^-. This fragment was also identified in DEA to taurine (see section above).

For the lowest collision energy in the lab frame (30 eV), the available energy is 16 eV, which lies above the resonance observed for this ion in DEA. Hence, from an energetic point of view, the formation of this fragment is allowed for all collision energies probed.

As discussed for DEA, contributions from both isobaric fragments have to be considered. The O^- point of origin may either be the S=O double bond cleavage or the hydroxyl (OH) group, where the H is attached to the neutral [T-O] fragment. NH_2^- may emerge from C-N single bond rupture.

$C_2H_2^-/CN^-$ (26 a.m.u.) and $C_2H_3^-/CNH^-$ (27 a.m.u.)

The 26 a.m.u. fragment has been identified in previous studies on electron transfer to alanine, valine and glycine [44, 69]. Due to the lack of reported isobaric information, one cannot differentiate between both assigned fragments and must

consider that the two contribute to the ion signal. Nevertheless, one should bear in mind that the electron affinity for CN (3.36 eV [61]) is much higher than that for C_2H_2 (0.49 eV [61]). The formation of either of the proposed ions requires multiple bond cleavage.

$C_2H_3^-/CNH^-$ represent the 26 a.m.u. anionic fragment with one more hydrogen atom. It is noteworthy the unique behaviour shown by this fragment, which is absent when the energy collision is decreased to 30 eV. It would be reasonable to think that $C_2H_2^-/CN^-$ could arise from the loss of one hydrogen atom from the fragment at 27 a.m.u., but given the absence of the latter for lower energies where $C_2H_2^-/CN^-$ is indeed present, the 26 a.m.u. ion probably does not originate (exclusively) from that path. It should be noted, however, that the absence of such anion in the experiment may also result from the fact that, due to the its low ionic yield, it may be hidden in the background signal, making its detection difficult.

This dissociation channel is biologically relevant since not only presupposes the loss of functionality of the amino acid, but also generates cyanide radical (CN^-), which is a highly reactive species. This compound has higher toxicity when compared to others. Indeed, it inhibits the enzyme cytochrome c oxidase preventing the ATP aerobic production, which can compromise the cell.

$NCO^-/CH_2CO^-/C_2H_4N^-$ (42 a.m.u.)

Three different molecular compounds can be assigned to the fragment detected at 42 a.m.u., contributing to one of the most intense peaks. As for other described fragments, in order to generate either of the listed anions several bond dissociations would have to occur.

In addition to bond cleavage, CH_2CO^- would also require substantial molecular rearrangement and formation of new bonds or new stable molecules. Despite that being also the case of NCO^-, its precursor (NCO) is a pseudo-halogen with high electron affinity (3.69 eV [61]) that exceeds those of halogen atoms, promoting the stabilization of the anion form. Furthermore, NCO^- has been pointed as a key fragment upon DEA and electron transfer to pyrimidine bases, formed through a complex decomposition process, which is expected to occur on longer time scales and in more than one step [45].

$C_2H_4N^-$ arises from loss of both hydrogen atoms attached to the nitrogen and from cleavage of the C-S bond.

On a relevant note, the equation used for the mass calibration of the spectra assigns the channel correspondent to the peak of this fragment to a 42.7 a.m.u..

From that, it would be reasonable to consider this fragment to be at 43 a.m.u.. Nevertheless, since the single possible negative ion with that *m/z* is CH_3CO^-, which has an electron affinity half of that for NCO^- (1.82 eV [61]), it is more likely that such discrepancy is due to a mass calibration error for higher masses.

$[T-N]^-/[T-CH_2]^-$ (111 a.m.u.)

This fragment formation has not been reported in free electron attachment experiments. Neither of the assigned molecular anions should be ruled out. However, the fragment $[T-CH_2]^-$ represents the complementary dissociative channel to the one yielding CH_2^-. Corroborating this fact, the branching ratios for $[T-CH_2]^-$ and CH_2^- have complementary behaviours: the relative cross section decreases from 30 to 70 eV and increases from 70 to 100 eV for the first, and the opposite is observed for the latter, i.e. increases from 30 to 70 eV and decreases from 70 to 100 eV. It is important to note that the changes in the relative cross section for the heavier fragment are more abrupt than that for the lighter one.

As mentioned above, assuming that the mass calibration shows some discrepancy in the high mass range, despite this fragment's peak appearing at 111 a.m.u., one should not discard the possibility of such anion being at *m/z* 110 a.m.u.. In that case, the negative ion is $[T-NH]^-$ and, from the intramolecular O−H···N hydrogen bond established between the amino and sulfonic groups, the corresponding neutral molecule would comprise one hydrogen from the amino (NH_2) group. Such dissociation mechanism is more likely to occur than the one that originates $[T-N]^-$, where the two hydrogen atoms pertaining to the amino group would have to be transferred to the neutral fragment upon dissociation of the C-N bond.

Other fragments

Apart from the fragmentation described above, five other fragment anions have been identified. While the formation of OH^- and H^- can result from single bond cleavage, the other species (C_2^-, C_2H^- and CH_2CN^-/C_2O^-) result from more complex molecular processes.

C_2H^- is one of the most prominent features in the TOF mass spectra. Despite the electron affinity of its neutral precursor being lower than that for C_2^- (2.97 and 3.97 eV, respectively), the relative cross section of the fragment 25 a.m.u. is higher than that of the fragment 24 a.m.u. and increases for higher collision energies.

OH^- has not been identified in DEA. On a first approach, it is fair to state that it originates from single OH-S cleavage. Again, the reported intramolecular hydrogen bond may ease such process.

In electron transfer studies a signal assigned to H^- is particularly evident for all three collision energies, being one of the most intense features in the spectra. Although the background spectra has been subtracted from the sample's signal, we do not discard the possibility of an artefact leading to an enhancement of such feature. Further studies with isotopic labelling would allow clarifying whether electron transfer mechanism enhances the formation of this fragment. Besides single bond cleavage, H^- can also originate from multi-step processes. As stated before, $H^\bullet$ is a free radical with high damage potential.

It is important to note that no $[T-H]^-$ is observed in potassium-taurine collisions. Such reaction is complementary to the formation of H^-. It seems that, if the loss of one hydrogen atom occurs leaving the rest of the molecule intact, the excess charge is only localised in the hydrogen fragment.

4.2.3 Discussion

The fragmentation pattern of taurine interaction with free electrons and potassium atoms has revealed to be significantly different. Only two fragments out of fifteen were observed in both experiments. The fragment masses 12, 13, 14, 17, 24, 25, 26, 27, 40, 42 and 111 a.m.u. have not been identified in free electron experiments and therefore information on the energy resonance profiles is not available. As such, it is not possible to draw significant conclusions as far as the differences between DEA and electron transfer mechanisms are concerned.

DEA to taurine led to four different fragments with relatively low intensity, in clear contrast with electron transfer results. Nonetheless, it appears that most fragment anions generated in both experiments arise from the amino side of the molecule, including the carbon chain, and not from the sulphur side. More than one (isobaric) negative anion is assigned for most *m/z* fragments detected. However, regarding the sequence of fragments from 24 to 42 a.m.u., resembles successive bond cleavages in taurine's carbon chain.

The significantly high dipole moment of taurine (15.5 D) seems to play a crucial role in the dissociation process of the molecule. As stated before, a high dipole moment leads to the existence of stable dipole-bound states, where the extra electron is trapped in a very diffuse orbital on the positive side of the dipole. These molecular states have been proven to be an intermediate state to electron capture to valence orbitals (through intramolecular electron transfer) that can lead

to dissociation. One of the requirements is the presence of a third body to help stabilize the complex against autodetachment.

Taurine's dipole moment being so high, the captured electron may lie in an orbital whose dimensions are far higher than that of the molecule, thus promoting autodetachment, unless a third body suppresses electron ejection from the temporary negative ion. This rationale justifies the reduced number of fragment anions in free electron attachment to taurine, where autodetachment may be the dominant process, in contrast with electron transfer, where the generated cationic potassium atom (K^+) stabilizes the TNI, enabling the access to dissociation channels.

Furthermore, since in such states the electron is localised in the positive side of the dipole, the accessed dissociative channels are expected to be mainly from that side of the molecule. Indeed, for this amino acid the positive side of the dipole corresponds to the amino end and the negative to the most electrophilic area of the molecule, which is the SO_3H end. The results presented here show that the damage is mainly induced in the amino side of the amino acid rather than the sulphur side, thus corroborating this rationale.

The formation of most of the herein reported fragment anions requires considerable internal rearrangement in the TNI and therefore the necessary energy may only be provided at high impact energies. Indeed, the branching ratios for such species, namely at 42 a.m.u., increase with increasing collision energy.

The fragments of mass 124 ($[T-H]^-$) and 46 a.m.u. are not detected in electron transfer experiments but are however detected in DEA. This can point to conclusion that formation of these negative ions in atom-molecule collisions is somehow suppressed in detriment of other fragments. The effects of free electrons can overestimate the relevance of the dehydrogenated parent anion. Indeed, one should not only consider the importance of this anion but perhaps even more important is the study of the fragmentation from main chain breaking. Some of these fragments can have quite high electron affinities and therefore can also be damaging agents to neighbouring molecular structures.

4.3 Thiaproline

L-4-Thiazolidinecarboxylic acid (thiaproline, TP) chemical structure ($C_4H_7NO_2S$) is depicted in figure 4.7. Its composition gives a total molecular weight of 133.2 g/mol (133 a.m.u.). Thiaproline is a proline ($C_5H_9NO_2$) analogue where the carbon atom from the position 4 of the ring is substituted by a sulphur atom.

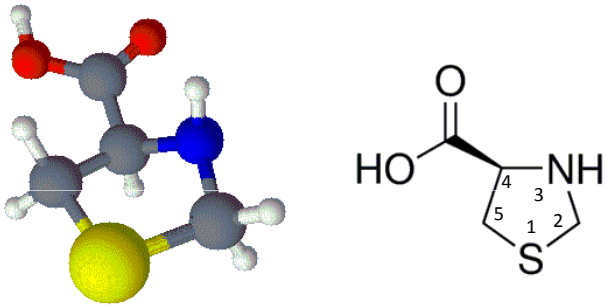

Figure 4.7: Schematic representation of thiaproline molecule: three-dimensional (left) and two-dimensional (right) models. White - hydrogen, black - carbon, blue - nitrogen, red - oxygen, yellow - sulphur.

4.3.1 Dissociative Electron Attachment Results

Low energy (<12 eV) electron impact on thiaproline in the gas phase produces several negatively charged fragments. They are tentatively ascribed by stoichiometry to the dehydrogenated thiaproline $[TP-H]^-$ (m/z 132), $[TP-O]^-$ (m/z 117), $[TP-CH_2N]^-$ (m/z 105), $[TP-SH]^-$ (m/z 100), $[TP-CO_2H]^-$ (m/z 88), $C_3O_2H_3^-$ (m/z 71), $SCNH_3^-$ (m/z 61), CH_2S^-/NS^- (m/z 46), CO_2H^- (m/z 45), $C_2H_4N^-/NCO^-$ / CH_2CO^- (m/z 42), S^- (m/z 32), $CN^-/C_2H_2^-$ (m/z 26), OH^- (m/z 17) and O^- (m/z 16). While the dehydrogenated parent anion and the fragments found at 117, 45, 17 and 16 a.m.u. may arise from direct single bond cleavage, the formation of the remaining fragments requires multiple bond cleavage and/or molecular rearrangement.

The energy dependences of the anionic fragments, or the anion yield functions, are plotted in figures 4.8 and 4.9. They exhibit structures indicative that the molecular dissociation proceeds through resonant mechanisms. The possible interpretations of the chemical composition for all labelled fragments is listed in table 4.6, along with the energy position for each resonance. For comparison purposes, in the referred table is presented a list of the fragments commonly found in previous studies of DEA to proline.

From the presented spectra it is possible to divide the resonance profiles in three main regions: one concerning structures found close to 0 eV incident electron energy, the second between 1 and 2 eV and the third in the 5-6 eV range. Additionally, few resonances were found at higher energies. Negative ions with similar resonance profiles suggest the presence of (1) close lying resonance states or (2) a pre-dissociative state. For the latter case, the extra electron can be trapped

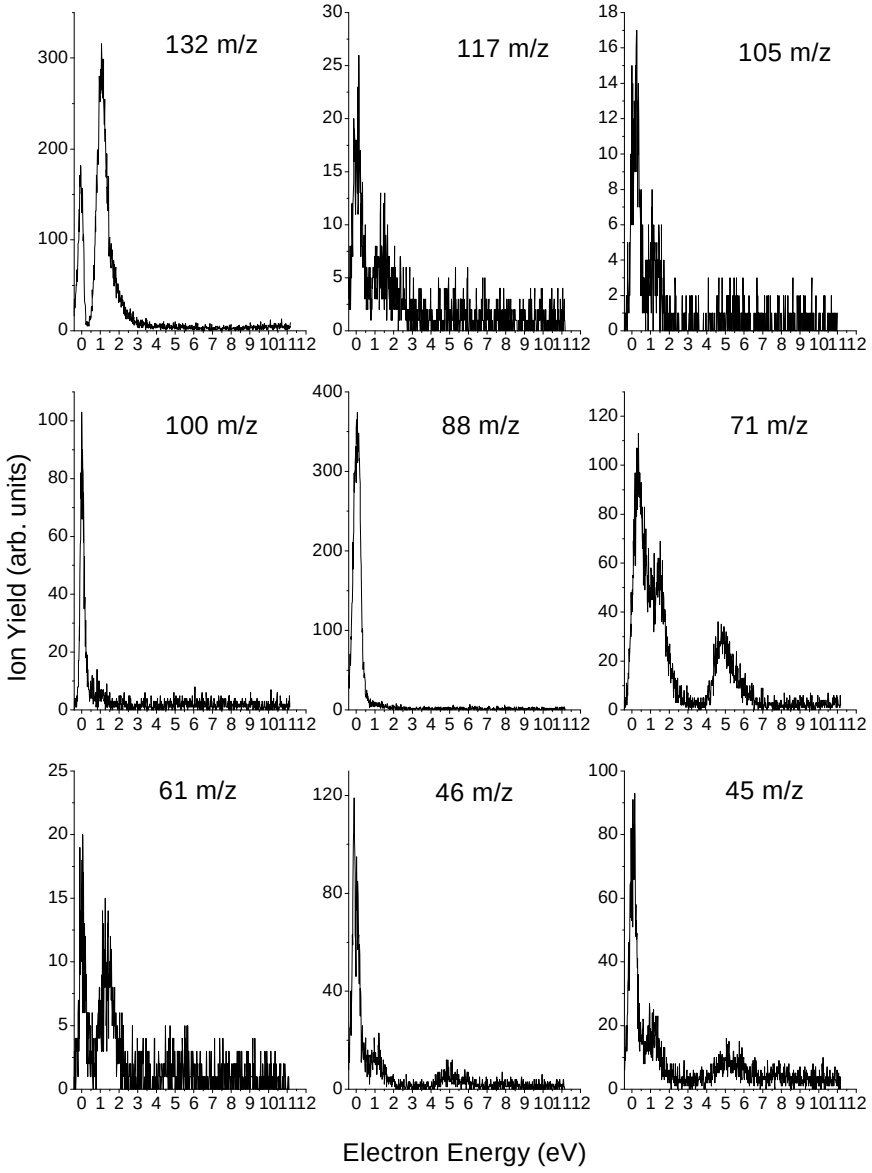

Figure 4.8: Ion yield of 132, 117, 105, 100, 88, 71, 61, 46 and 45 *m/z* as a function of the incident electron energy. Possible chemical compositions of these fragments are given in table 4.6

by the molecule creating a TNI that decays along the repulsive potential energy surface up to a point where different dissociative channels may become accessible. In other words, the similar resonance profiles imply that, while the initial accessed state may be the same, it then opens up different fragmentation pathways.

In addition, resonant features in the 1-2 eV range may also be initiated from the pre-dissociative -COOH (carboxylic group) π^* states found for most amino acids, including proline [72].

As for most biologically relevant molecules, such as amino acids and DNA

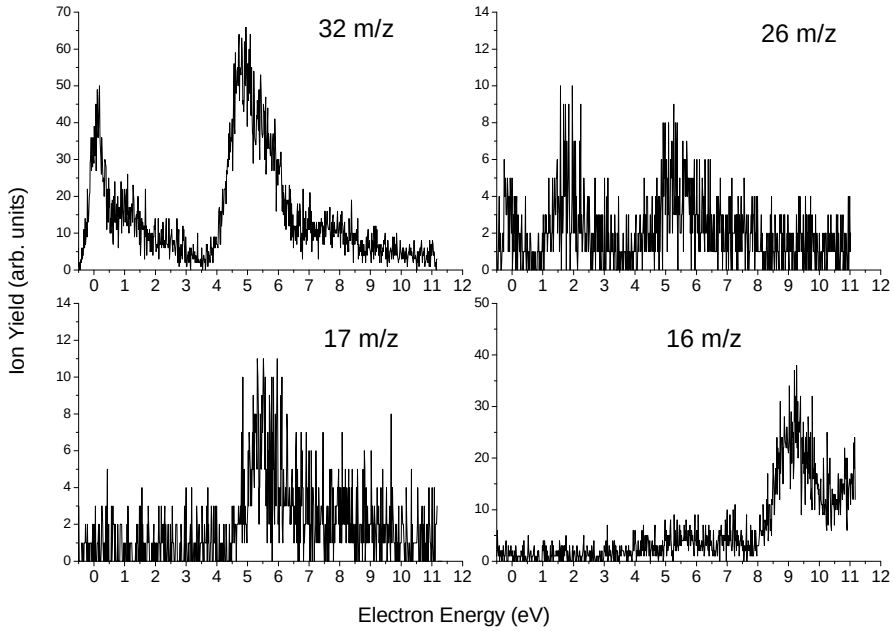

Figure 4.9: Ion yield of 32, 26, 17 and 16 *m/z* as a function of the incident electron energy. Possible chemical compositions of these fragments are given in table 4.6

bases, also in thiaproline the most abundant anion yield is observed for neutral H-loss. Dehydrogenation of thiaproline for the production $[TP-H]^-$ negative ions is most likely to occur at the carboxylic group via a single O-H bond rupture. It has been shown for glycine [73] that the COOH site is the most sensitive to electron attack. However, H-loss from other sites such as amino and carbon atoms, should not be discarded.

Two clear structures are present in $[TP-H]^-$ ion yield: one at 0 eV and the other at around 1 eV. It is known that acetic acid [74], which possesses a carboxylic group but no amino group, shows only one resonance at 1 eV, while DEA to valine [40] resulting in $[Valine-H]^-$ shows mainly two resonances, one at about 1 eV and another at 5 eV. This suggests that, for thiaproline the resonance found at 1 eV can be assigned to the H-loss from the O-site. Considering the thermodynamic threshold for the fragment ion formation to be 0.6 eV (concerning the resonance at 1 eV) and the bond dissociation energy D(O-H) = 4.4 eV [61], one can anticipate the value for the electron affinity of [TP-H] radical to be 3.8 eV.

The resonance at 0 eV may arise from N-H or C-H single bond rupture, or from a more complex multi-step mechanism. Nevertheless, resonances at 1.2 and 5.3 eV were reported in DEA to proline[70, 71] but none was found at 0 eV. As such, it is reasonable to state that the sulphur atom present in the molecule ring allows access to different dissociation channels. On a relevant note, since the peak at 1

Table 4.6: Resonance positions of the anionic fragments generated from DEA to thiaproline and comparison with previous results of DEA to proline.

Ion	*m/z*	Electron energy (eV)				Proline
$[TP-H]^-$	132	0	1.1			[70, 71]
$[TP-O]^-$	117	0.1	1.3			-
$[TP-CH_2N]^-$	105	0.2	1.2			-
$[TP-SH]^-$	100	0				-
$[TP-CO_2H]^-$	88	0				-
$C_3O_2H_3^-$	71	0.4	1.4	5.0		[71]
$SCNH_3^-$	61	0.1	1.4			-
CH_2S^-	46	0	1.0	5.0		-
CO_2H^-	45	0.1	1.1	5.2		[70, 71]
$C_2H_4N^-/NCO^-/CH_2CO^-$	42			5.6	7.6	-
S^-	32	0.1	1.0	5.0	7.7	-
$CN^-/C_2H_2^-$	26	0	1.8	5.5		[70, 71]
OH^-	17			5.7		[70, 71]
O^-	16			5.5	9.2	[70, 71]

eV has a steep onset but is rather broad on the high energy side, it is possible that other features with low intensity may be contributing for such broadening. A better resolution of the apparatus is required to clarify.

Two resonances are visible for the fragment at mass 16. It is more likely it is related to O^- rather than NH_2^-, given the different electron affinities (1.5 and 0.7 eV, respectively) and the more complex reaction needed to generate NH_2^-. The formation of O^- proceeds via the rupture of the C=O bond and/or through the cleavage of both C-O and O-H bonds at the carboxylic group. In the first case, the thermodynamic threshold for the ion formation is estimated to be 4.2 eV (D(C=O)=5.7 eV, EA(O)=1.5 eV), which lies below the experimental appearance energy (4.8 eV). This reaction can be seen as the complementary reaction to the 117 mass formation, where $[TP-O]^-$ should be the dominant anion. Nonetheless, the resonance spectra of both fragments do not show any similarity, which means that the accessed dissociation channels must be different in the two cases.O^- has been also reported in free electron attachment to proline, with resonance profiles at high energies (6.2 and 10.2 eV), slightly higher than for thiaproline.

Two other complementary dissociative reactions pertain to the formation of fragments at masses 88 ($[TP-CO_2H]^-$) and 45 (CO_2H^-). The same holds for formation of $C_3O_2H_3^-$ (*m/z* 71) and $SCNH_3^-$ (*m/z* 61).

The first case yields one of the most dominant fragments ($[TP-CO_2H]^-$), together with the dehydrogenated parent anion, as a sharp resonance at 0 eV. The

production of this fragment and of CO_2H^- results from cleavage of the single C-C bond, separating the carboxylic group (45 a.m.u.) from the ring (88 a.m.u.). The ion yield functions of both fragments show a peak at 0 eV, suggesting that they may originate from the same dissociation channel, but $COOH^-$ shows two other resonances with lower intensity at around 1 and 5 eV. This ion has been reported in electron attachment to proline, with resonances at around 3, 5 and 8 eV [70, 71].

Thermodynamic threshold calculations for $COOH^-$ are in agreement with the experimental appearance energies. If the dissociation proceeds via a single rupture of the C-C bound, the appearance energy is estimated to be 2.8 eV (D(C-C)=6.3 eV, EA(COOH)=3.5 eV [61]), which lies below the resonance centred at 5.2 eV. A concerted reaction which requires substantial displacement of the hydrogen atom has been reported in DEA to proline studies [70]. The authors suggest that the fragment may arise from cleavage of the C-C bond at the carboxylic group concomitantly to the swing over of the hydrogen atom from the oxygen site to the carbon position. This reation is endothermic by 0.6 eV, in good agreement with the experimentally observed threshold for detection of the anion related to the near 1 eV resonance (~0.6 eV).

Anionic complementary fragments at *m/z* 71 ($C_3O_2H_3^-$) and *m/z* 61 ($SCNH_3^-$) have very similar yield functions, indicating that the same dissociation channel is accessed. The two emerge from S-C(5) and N-C(4) bond ruptures, with an extra H-loss in the mass 71 case. Sulzer *et. al* [71] also reported a 71 a.m.u. negative ion for proline, although in that case the fragment is ascribed to $[Proline - CO_2]^-$.

Sulphur containing neutral and anionic fragments were found in the presented results. S^- for example, despite not being the most prominent fragment, has at least four resonances. The broad peak at around 5 eV can comprise more than one resonance, but better energy resolution is required to clarify. Fragment $[TP - SH]^-$ yield function shows a sharp peak at 0 eV incident electron energy and generates neutral S and/or SH counterparts. The aforementioned anionic fragments cause the ring to break, thus implicating complete loss of functionality from the molecule.

Sulzer *et al.* [71] concluded that DEA to proline exclusively leads to the formation of $C_2H_2^-$ in the region of 26 *m/z*, as the very low yields of CN^- at lower energies are related to background contributions. However, in the present results there is not enough information to rule out the CN^- contribution to the 26 *m/z* signal.

Another fragment anion that can basically be generated by a single bond cleavage at the carboxylic group is the OH^- ion. It was observed only through one resonance centred at 5.7 eV. The thermodynamic threshold is estimated to be

$AE = D(C-OH) - EA(OH) = 4.0 - 1.83 = 2.17$ eV. Since the reaction occurs at 4.5 eV, it can, indeed, result from a single bond cleavage leaving the rest of the molecule unchanged.

As stated before, anion formation in the energy range below 4 eV is typically associated with shape resonances. Above 5 eV fragments are usually formed via core-excited resonances. Although no dipole moment values for thiaproline were found in the literature, one should not discard the possibility of electron capture through dipole-bound states. Indeed, sharp resonances peaking at 0 eV, such as the ones found for *m/z* 132, 100, 88 and 45, are characteristic of vibrational Feshbach resonances associated with high dipole moments.

4.3.2 Electron Transfer Results

Thiaproline molecules were made to collide with neutral potassium atoms with kinetic energies of 12, 17, 30, 50, 70 and 100 eV. The negative ion TOF mass spectra obtained for 30, 70 and 100 eV collision energies in the lab frame are presented in figure 4.10. Fifteen different fragment anions were identified and labelled from A to O. Peak assignments are listed in table 4.7, along with those found in DEA results. Additionally, branching ratios for the major fragments as a function of the collision energy are shown in figure 4.11.

A brief analysis of these data shows that the most abundant fragments are assigned to SH^- (*m/z* 33), followed by O^- (*m/z* 16), OH^- (*m/z* 17), S^- (*m/z* 32) and the dehydrogenated parent anion $[TP-H]^-$ (*m/z* 132).

A close inspection of table 4.7 reveals that DEA and electron transfer to thiaproline yield eight fragments with the same mass and composition. Concerning the quantity of anionic fragments generated, both processes yield 14 and 15, respectively. Hence, the two dissociative mechanisms appear to be equally effective in inducing dissociation and to proceed through similar fragmentation pathways. Regarding the composition of the ions, it seems that DEA is able to generate heavier molecular anions than electron transfer process, most likely due to the higher available energy transferred from the potassium atom to the molecule in the collision process.

Collision energies of 12 and 17 eV in the lab frame correspond to available energies of 3.92 and 7.36 eV, respectively (table 4.1). Taking into account that dissociative channels accessed through electron transfer may be the same as for DEA, one can tune the electron donor collision (kinetic) energy to selectively access a given channel (resonance) found in DEA. This means that, at 17 eV collision energy, dissociative channels associated to DEA resonances located above 7.36

Table 4.7: Assigned anionic fragments in DEA and electron transfer to thiaproline.

		Electron transfer						
Anionic Fragments	*m/z*	12 eV	17 eV	30 eV	50 eV	70 eV	100 eV	DEA
Metastable decay	15.5	-	A	A	A	A	A	-
O^-/NH_2^-	16	-	-	B	B	B	B	✓
Metastable decay	16.5	-	-	C	C	C	C	-
OH^-	17	-	-	D	D	D	D	✓
C_2^-	24	E	E	E	E	-	E	-
C_2H^-	25	-	-	F	F	F	F	-
$C_2H_2^-/CN^-$	26	-	-	-	G	G	G	✓
HNO^-	31	-	-	H	H	-	-	-
S^-	32	-	I	I	I	I	I	✓
SH^-	33	-	J	J	J	J	J	-
$H_3O_2^-$	35	-	K	K	K	K	K	-
$NCO^-/C_2H_4N^-$	42	-	-	-	L	L	L	✓
CO_2H^-	45	-	-	-	M	M	M	✓
$CO_2H_2^-/CH_2S^-/NS^-$	46	-	-	-	N	N	N	✓
$SCNH_3^-$	61	-	-	-	-	-	-	✓
$C_3O_2H_3^-$	71	-	-	-	-	-	-	✓
$[TP-CO_2H]^-$	88	-	-	-	-	-	-	✓
$[TP-SH]^-$	100	-	-	-	-	-	-	✓
$[TP-CH_2N]^-$	105	-	-	-	-	-	-	✓
$[TP-O]^-$	117	-	-	-	-	-	-	✓
$[TP-H]^-$	132	O	O	O	O	O	O	✓

eV will not be accessed. Furthermore, at 12 eV collision energy only resonances located below 3.92 eV will be accessed.

Electron transfer to thiaproline measurements at 12 and 17 eV potassium collision energies were performed with the purpose of selecting certain DEA resonances. At 12 eV for example, dissociative channels leading to the formation of OH^- and O^- would not be accessed, since both fragments have resonances above 3.92 eV (see table 4.6). The most prominent feature related to S^- formation would not be accessed as well.

The neutral potassium beam reaching the collision region with such collision energies has very low intensity. Significantly long acquisition times are required in order to acquire a spectrum with a signal-to-noise ratio that allows to discriminate the fragments peaks.

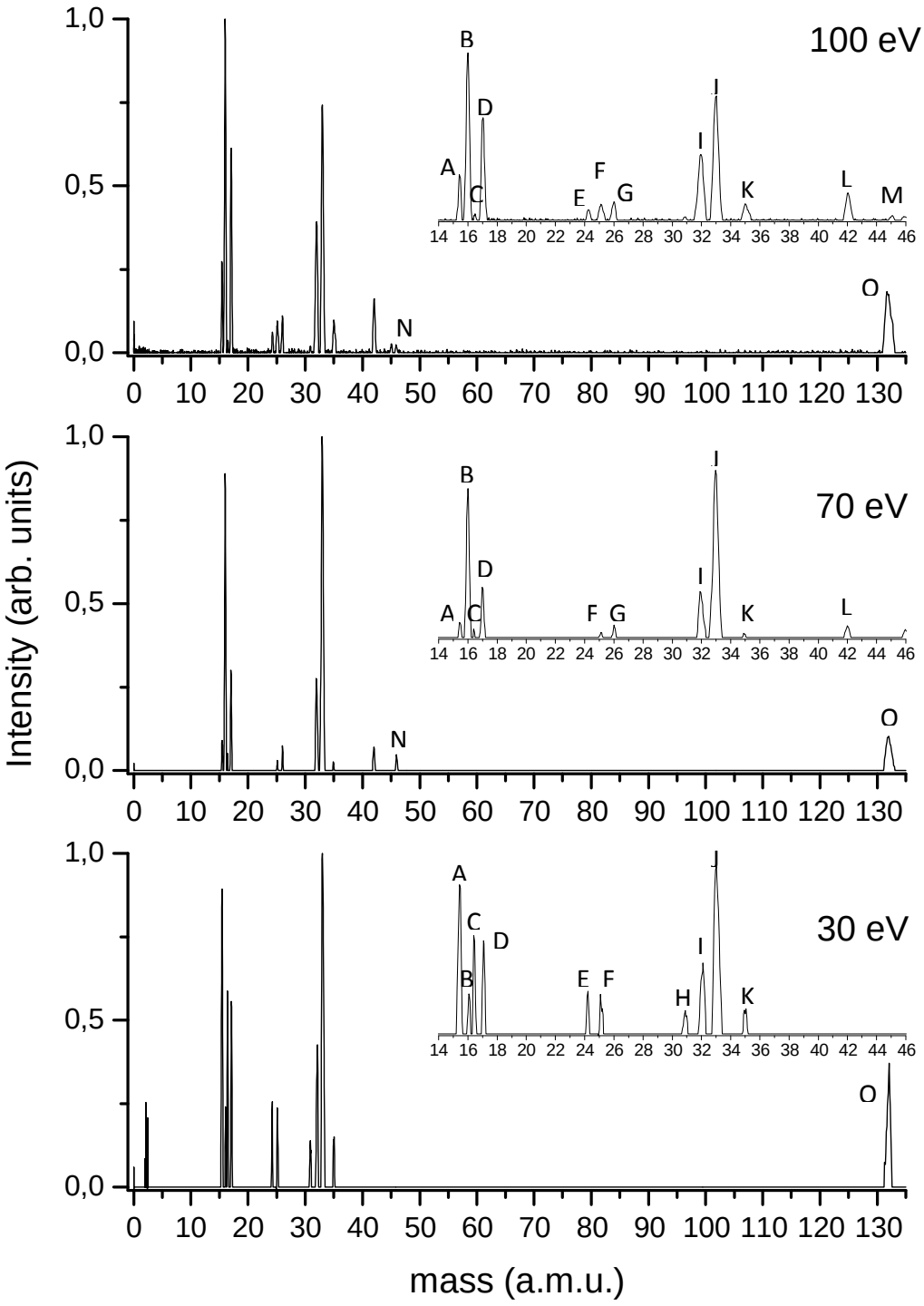

Figure 4.10: Thiaproline TOF anion spectra at 30, 70 and 100 eV collision energies.

The obtained spectra for 12 and 17 eV do not have a signal-to-noise ratio good enough to draw significant and irrefutable conclusions concerning the relation between electron transfer and DEA promoted dissociative channels. Nevertheless, the formation of the fragments $[TP-H]^-$ and C_2^- is clear at 12 eV. Since S^-, SH^-, OH^- and O^- have more prominent peaks than $[TP-H]^-$ and C_2^- at higher collision energies, and no structures associated with these fragments are observed at 12 eV, one can argue that its formation is indeed diminished, if not completely absent. Noting that fragments at masses 32, 33, 17 and 16 exhibit resonant features at around 5 and 7 eV, the results appear to corroborate the assumption that DEA and electron transfer mechanisms may promote the same dissociative channels.

Furthermore, for 17 eV collision energy S^-, SH^-, and the dehydrogenated parent anions are identified, whereas no significant peak associated with O^- is observed. In fact, while the most intense resonance associated with S^- is below the available energy, that for O^- is above, and thus is not accessed.

Measurements conducted for collision energies above 30 eV allow, from an energetic point of view, the access to all dissociative pathways documented for DEA to thiaproline. As for taurine, branching ratios for most fragment anions vary with the collision energy, suggesting that the access to a dissociative channel is also dependent on the collision time scale (higher energies mean lower collision time).

$[TP-H]^-$ (132 a.m.u.)

In this experiment, although present at all collision energies, the dehydrogenated parent anion is not one of the most abundant fragments, in contrast with DEA results. The relative cross sections for this fragment formation show a unique behaviour, where, despite showing minor variations, it may be seen as relatively constant with increasing energy.

As reported for several other molecules, including the amino acids alanine and valine [44], one would expect that the relative cross section for the dehydrogenated parent formation would decrease for increasing collision energies. Higher collision energies mean higher energy transferred to the molecule, which may promote different dissociative channels. It may also happen that this fragment being generated with excess internal energy may in turn dissociate into other lighter fragments, originating the so-called metastable decays. The fact that this anion is observed at all collision energies is in agreement with the DEA results, since all three resonances reported are accessed. As stated before, the formation

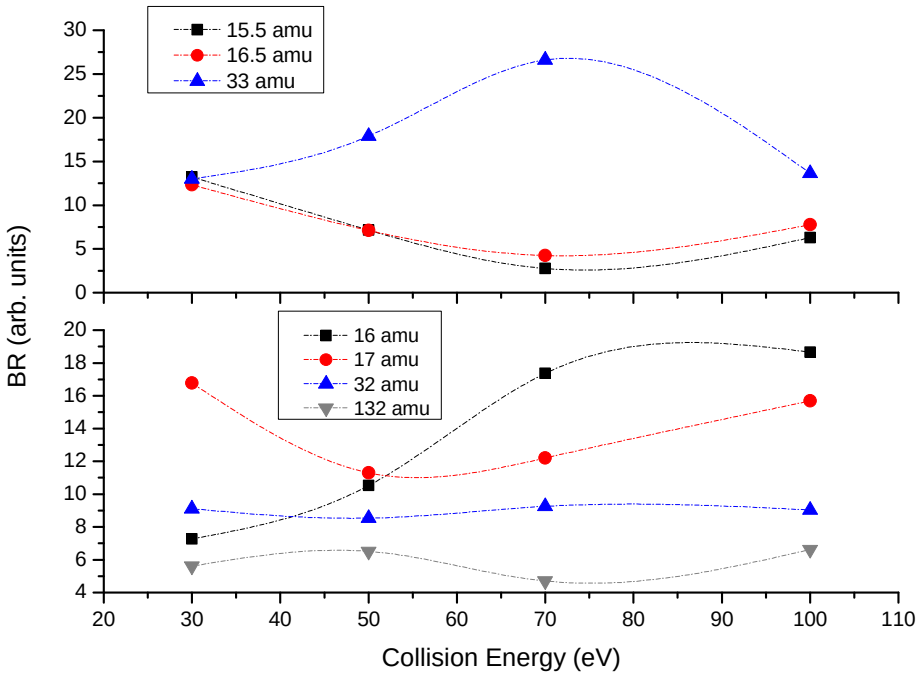

Figure 4.11: Thiaproline relative cross section.

of the dehydrogenated parent anion may arise from the capture of the electron by a π^* orbital from the carboxyl group, which couples with a σ^* orbital leading to dissociation of the O-H bond. Such pathway has been proposed in theoretical studies by Rescigno *et al.* [75] for carboxylic acids, such as formic acid.

This reaction is relevant from a biological point of view, since it implies the formation of a neutral highly reactive free radical species, $H^{\bullet}$.

SH^- (33 a.m.u.) and S^- (32 a.m.u.)

SH^- is the most intense fragment anion in the present experiment at all collision energies probed, except for 12 and 17 eV, while S^- intensity is around half of that for SH^-.

Two S-C bonds have to cleave in order for S^- to be formed. In the SH^- case, besides the same S-C bond cleavage, a molecular rearrangement resulting in an hydrogen atom transfer to the sulphur site as to occur. Intuitively, one could say that more energy is required to generate the anion at 33 *m/z*. However, four stable low energy conformers of thiaproline have been reported [76], where, in one of them, an hydrogen bond between the hydroxyl group and the sulphur atom (O−H···S) takes place. This hydrogen bond may promote the SH anion formation.

In addition, the relatively high electron affinities of the two neutral precursors (EA(SH)=2.31 eV, EA(S)=2.08 eV [61]) may also promote its formation.

Interestingly, no SH^- as been detected in free electron attachment, which can suggest that there is a stabilization effect achieved by the presence of the potassium cation. It is plausible that the dissociative channel yielding SH^- may be the same as for S^-, since neither of the fragments seem to be absent in the TOF mass spectrum probed at 17 eV.

As far as branching ratios concern, SH^- has the higher relative cross section which shows a significant increase from 30 up to 70 eV, decreasing at 100 eV, while S^- seems to have a relatively constant cross section throughout the different collision energies.

From a biological point of view, SH corresponds to sulfanyl radical, which can react with O_2 producing SO_2^-, which in turn can further react with O_2 to make the highly toxic superoxide O_2^-.

O^- (16 a.m.u.) and OH^- (17 a.m.u.)

In DEA experiments O^- and OH^- had small contributions when compared to other fragments. Only resonances above 5 eV (core-excited resonances) are associated with these fragments formation. Thus, despite being almost insignificant, the feature found at *m/z* 16 in the 12 eV spectrum is most likely associated with the presence of residual gas in the high vacuum chamber.

From figure 4.11 is clear that O^- formation ratio significantly increases with increasing collision energy (from 30 to 100 eV), and OH^- relative cross section decreases from 30 to 50 eV, increasing thereafter.

Other fragments

It is noteworthy that the presence of fragments at 45 a.m.u. (CO_2H^-) and 46 a.m.u ($CO_2H_2^-/CH_2S^-/NS^-$) is quite less significant in electron transfer experiments when compared to free electron attachment, even more considering that COOH formation "only" requires a single C-C bond cleavage. Its formation in atom-molecule collisions is somehow suppressed in detriment of other fragments. Furthermore, COOH appears to be formed only for energies higher than 50 eV, and the same holds for *m/z* 46. However, given the low intensity signal of these fragments, its features may be hidden in the background noise for lower energies.

A low intensity structure observed at *m/z* 31 is found for 30 and 50 eV. This fragment has been assigned by stoichiometry to HNO^-. Its formation requires a

considerable molecular rearrangement, and its electron affinity (EA(HNO)=0.33 eV [61]) may not be enough to promote this reaction pathway. Thus, one should not rule out the hypothesis that this fragment may arise from a multi-step complex reaction or from the background.

Metastable decays

Two prominent peaks are associated with fragments with *m/z* 15.5 and 16.5. Since the peaks corresponding to O^- and OH^- are well defined and centred at *m/z* 16.0 and 17.0 respectively, these two peaks do not arise from mass calibration error. Instead, they should probably result from metastable decay of the dehydrogenated parent anion during his time of flight.

The assessment of the relative cross section values of *m/z* 15.5 and 16.5 can suggest that these fragmentation channels arise from populating the same initial anionic state, since the cross sections are practically the same and show similar behaviour. Perhaps more relevant is the fact that these branching ratios show the exact opposite (complementary) behaviour to the one pertaining to SH^- formation. From that, one can state that the fragments probably represent SH^- formation through metastable decay of the dehydrogenated parent anion, i.e. $[TP-H]^-$ may be formed with excess energy and along his time of flight may further dissociate and generate other smaller fragments, such as SH^-. If an anion is generated in other site rather than the collision region, the time of flight of such fragment is misread, as is the case of the metastable fragments at 15.5 and 16.5 *m/z*.

The branching ratios of metastable and SH^- anions show that at 30 eV both pathways for SH^- formation are more competitive than for higher energies, where the direct formation of this ion is dominant.

4.3.3 Discussion

The fragmentation patterns of thiaproline with free electrons and potassium atoms are quite similar in terms of quantity of fragments produced. A total of 14 and 15 anions were detected in DEA and electron transfer respectively, from which eight are formed through the two mechanisms. However, free electron attachment seems to yield heavier fragment than electron transfer in atom-molecule collisions. Indeed, no fragments between 42 and 132 masses are observed in the latter process, in contrast with the first. This has to due with the higher energy transfer inherent to the collision energies involved in atom-molecule experiments.

From the acquired TOF mass spectra at 12 and 17 eV, it seems that the dissociative channels accessed in DEA yielding the fragments O^-, OH^- and S^- are the same for electron transfer.

Comparing previous DEA to proline studies [70, 71] with the data here presented for thiaproline, we evidence crucial differences in the molecule fragmentation pathways. The ascribed fragment anions for proline are suggested to arise mostly from the carboxylic group, whereas for thiaproline the damage appears to be mostly induced to the ring, more specifically to the sulphur site.

In addition, the resonance profiles for fragments found both in proline and the sulphur containing analogue are clearly different. This suggests that the sulphur atom effectively changes the accessed dissociative channels and thus the fragmentation pathways of the molecule upon electron attachment.

Chapter 5

Conclusions and Future Work

5.1 Conclusions

The main emphasis of this thesis is to study negative ion formation triggered by free electron attachment and electron transfer to two sulphur containing molecules of biological relevance, namely taurine and thiaproline.

Results of induced fragmentation of taurine by free electrons are markedly different from those obtained upon potassium-taurine collisions. DEA to this sulphur containing amino acid generated four anionic fragments with relatively low intensity, while electron transfer measurements revealed thirteen.

It is suggested that the considerably high dipole moment of this molecule plays a crucial role in the dissociative reactions. In fact, it may promote autodetachment of the captured electron unless a third body is present to stabilize the complex and allow enough time for the dissociative channels to be accessed. A successful competition between dissociation and autodetachment is required and achieved in the probed electron transfer measurements where a third body (K^+) is indeed present. The cationic potassium allowed significant dissociation of the molecule through dissociative channels not accessed in DEA. On the other hand, most damage was found to be induced in the amino side (positive pole) and carbon chain of the molecule (CNO^- and $C_2H_2^-$ are two examples). Since the electron is most likely captured in the positive side of the dipole, the accessed channels may be limited to that side.

It is also noteworthy that no dehydrogenated parent anion was found in electron transfer experiments, but is the second most intense fragment in DEA with three resonances at 0, 1.1 and 1.7 eV. From an energetic point of view, for the probed collision energies all resonances observed in DEA could be accessed in electron transfer.

The sulphur atom is part of the SO_3H side the molecule, which, because of the comprised oxygen and sulphur atoms, is a highly dense and negatively charged pole, compared to the amino side or positive pole. Hence, one may state that the sulphur atom has an indirect role in the dissociation process, since it is the core of the high dipole moment of this amino acid.

DEA and electron transfer mechanisms were found to be equally effective in damaging thiaproline. A manifold of fragments were detected, with half being commonly generated in both experiments.

The resonant profiles were found in three main energy regions: at 0 eV, 1-2 eV and 5-6 eV. Sharp resonances at 0 eV indicate shape or vibrational Feshbach resonances while above 4 eV are typically core-excited resonances. The carboxylic group (COOH) is efficiently separated from the molecule by electrons with energies ranging from 0 to 5 eV, with the extra charge being located in either fragment. The sulphur anion is formed by two S-C bonds cleavage, through at least four different resonances.

Electron transfer to thiaproline, in addition to S^-, yields SH^- as the most prominent fragment. The coulombic interaction within the collision complex allows for this anion to be formed, where most likely the hydrogen from the hydroxyl group is transferred to the excised sulphur atom. When compared to free electron induced fragmentation, electron transfer promotes the formation of lighter anions.

Collision energies at 12, 17, 30, 50, 70 and 100 eV were probed. The first two were chosen according to the information provided on the resonances by the DEA experiments. Indeed, despite the weak signal-to-noise ratio, the formation of S^-, SH^- and O^- appears to be associated with the access to a specific initial TNI resonant state.

The role of the sulphur atom in the fragmentation process can be easily assessed by comparing the present results with previous DEA to proline. By doing so, it is clear that not only the anionic fragments are quite different but also the resonance profiles for ions with the same mass found for both molecules do not agree with each other. This suggests that the sulphur atom alters the accessed channels and thus the fragmentation pathways. It is important to note that the damage induced to thiaproline appears to be centred in the ring, which is even more noticeable in electron transfer, while for proline most fragments seem to arise from the carboxylic group.

It is noticeable that the presence of the sulphur atom within thiaproline controls the fragmentation pathways, as this seems to occur mainly through the sulphur site of the molecule, specially in electron transfer experiments. The present results

demonstrate that certain reactions can be controlled by substitution of sulphur at specific molecular sites.

From a biological point of view, the here presented results are relevant in the nuclear medicine and radiotherapy fields. Upon dissociation through the described pathways, the studied molecules would loose its functionality. Moreover, the generated anionic fragments have the capability to react in the cellular medium causing bond ruptures or originating other species. From the reported anions, the most relevant is the cyanide anion (CN^-), known for its high toxicity. Furthermore, some of the anionic fragments imply the formation of neutral radical and highly reactive species such as $H^\bullet$, $O^\bullet$ and $OH^\bullet$, being these related to oxidative stress.

From a more fundamental perspective, one can argue that given the electron transfer mechanism ability to lower autodetachment rates and therefore enhance fragmentation channels, these processes may have a more damaging effect on biological molecules than DEA. In this study, the relevance of the presence of a third body is highlighted and some similarities with electron carriers in the biological medium can be discussed.

5.2 Future Work

For future work it would be interesting to conduct theoretical calculations of equilibrium geometrical structures of the neutral species, as well as for lowest unoccupied molecular orbitals (LUMO's), and compare with the DEA and electron transfer experimental results to better assess the dissociation mechanisms. Theoretical calculations using the Schwinger Multichannel (SMC) method are already being performed by Prof. Márcio Bettega and his colleagues at UFPR.

Further investigation on isobaric fragments would allow the assignment of a single fragment to a respective mass. Such studies would be more relevant for the many possible stoichiometric compositions ascribed to taurine fragments. Sulzer *et al.* [71] are able to separate isobaric fragments with their apparatus' high mass resolution. The Innsbruck group would be also able to assess the origin of the metastable decays found for thiaproline, through their double focusing two sector field spectrometer.

Furthermore, labelling hydrogen sites with methyl groups for example, would allow the identification of the H^- fragment origin from taurine.

It would be relevant to conduct electron transfer experiments to proline and compare with the present thiaproline data.

Other derivatives of thiaproline, where the carboxylic group is attached to the

carbon in the position 2 at the ring rather than 4, could be interesting to measure and compare with the present results.

As far as the set-up concerns, the installation of an energy analyser to measure the energy loss of the potassium after collision with the molecular beam would allow to draw further significant conclusions in what concerns the formation energy of each detected fragment, as well as the accessed states in the electron transfer process.

Bibliography

[1] C. Sonntag. *The chemical basis of radiation biology*. Taylor & Francis London, 1987.

[2] I. Baccarelli, I. Bald, F. A. Gianturco, E. Illenberger, and J. Kopyra. "Electron-induced damage of DNA and its components: Experiments and theoretical models". In: *Physics Reports* 508.1 (2011), pp. 1–44.

[3] H. Varmus. "The new era in cancer research". In: *Science* 312.5777 (2006), pp. 1162–1165.

[4] E. Brun, P. Cloutier, C. Sicard-Roselli, M. Fromm, and L. Sanche. "Damage induced to DNA by low-energy (0- 30 ev) electrons under vacuum and atmospheric conditions". In: *The Journal of Physical Chemistry B* 113.29 (2009), pp. 10008–10013.

[5] L. Sanche. "Low energy electron-driven damage in biomolecules". In: *The European Physical Journal D-Atomic, Molecular, Optical and Plasma Physics* 35.2 (2005), pp. 367–390.

[6] E. Alizadeh and L. Sanche. "Precursors of solvated electrons in radiobiological physics and chemistry". In: *Chemical reviews* 112.11 (2012), pp. 5578–5602.

[7] G. B. Elion. "The purine path to chemotherapy". In: *Science* 244.4900 (1989), pp. 41–47.

[8] B. Boudaıffa, P. Cloutier, D. Hunting, M. A. Huels, and L. Sanche. "Resonant formation of DNA strand breaks by low-energy (3 to 20 eV) electrons". In: *Science* 287.5458 (2000), pp. 1658–1660.

[9] E. Illenberger and J. Momigny. *Gaseous Molecular Ions: An Introduction to Elementary Processes Induced by Ionization*. Topics in Physical Chemistry. Steinkopff, 2012.

[10] J. Aldrich, K. Lam, P. Shragge, and J. Hunt. "Fast electron reactions in concentrated solutions of amino acids and nucleotides". In: *Radiation research* 63.1 (1975), pp. 42–52.

[11] F. Martin, P. D. Burrow, Z. Cai, P. Cloutier, D. Hunting, and L. Sanche. "DNA Strand Breaks Induced by 0–4 eV Electrons: The Role of Shape Resonances". In: *Physical review letters* 93 (6 2004), p. 068101.

[12] G. Hanel, B. Gstir, S. Denifl, P. Scheier, M. Probst, B. Farizon, M. Farizon, E. Illenberger, and T. D. Märk. "Electron Attachment to Uracil: Effective Destruction at Subexcitation Energies". In: *Physical review letters* 90 (18 2003), p. 188104.

[13] S. Lehnert. "Biomolecular action of ionizing radiation". In: *Biomolecular Action of Ionizing Radiation. Series: Series in Medical Physics and Biomedical Engineering. Taylor & Francis, Edited by Shirley Lehnert* 1 (2007).

[14] S. Ptasińska, S. Denifl, V. Grill, T. D. Märk, E. Illenberger, and P. Scheier. "Bond-and site-selective loss of H-from pyrimidine bases". In: *Physical review letters* 95.9 (2005), p. 093201.

[15] S. Ptasinska, S. Denifl, P. Scheier, E. Illenberger, and T. D. Märk. "Bond-and Site-Selective Loss of H Atoms from Nucleobases by Very-Low-Energy Electrons (< 3 eV)". In: *Angewandte Chemie International Edition* 44.42 (2005), pp. 6941–6943.

[16] S. Ptasińska, S. Denifl, B. Mróz, M. Probst, V. Grill, E. Illenberger, P. Scheier, and T. Märk. "Bond selective dissociative electron attachment to thymine". In: *The Journal of chemical physics* 123.12 (2005), p. 124302.

[17] S. Ptasińska, S. Denifl, V. Grill, T. D. Märk, P. Scheier, S. Gohlke, M. A. Huels, and E. Illenberger. "Bond-Selective H- Ion Abstraction from Thymine". In: *Angewandte Chemie International Edition* 44.11 (2005), pp. 1647–1650.

[18] A. D. McNaught and A. D. McNaught. *Compendium of chemical terminology*. Vol. 1669. Blackwell Science Oxford, 1997.

[19] I. Bald, J. Kopyra, and E. Illenberger. "Selective Excision of C5 from D-Ribose in the Gas Phase by Low-Energy Electrons (0–1 eV): Implications for the Mechanism of DNA Damage". In: *Angewandte Chemie International Edition* 45.29 (2006), pp. 4851–4855.

[20] J. F. Wishart and B. M. Rao. *Recent trends in radiation chemistry*. World Scientific, 2010.

[21] R. Antunes, D. Almeida, G. Martins, N. Mason, G. Garcia, M. Maneira, Y. Nunes, and P. Limão-Vieira. "Negative ion formation in potassium–nitromethane collisions". In: *Physical Chemistry Chemical Physics* 12.39 (2010), pp. 12513–12519.

[22] M. J. d. P. Maneira. "Formação de pares de iões em colisões entre átomos e moléculas tetraédricas". PhD thesis. New University of Lisbon, 1984.

[23] A. Kleyn and A. Moutinho. "Negative ion formation in alkali-atom-molecule collisions". In: *Journal of Physics B: Atomic, Molecular and Optical Physics* 34.14 (2001), R1.

[24] P. Limão-Vieira. "Fragmentação de iões negativos de halobenzenos induzida por colisão". In: *UNL, Lisboa* (1999).

[25] A. W. Kleyn. "Vibronic excitation in atom molecule collisions". PhD thesis. 1980.

[26] R. A. F. Antunes. "The role of halouracils in radiotherapy studied by electron transfer in atom-molecule collisions experiments". PhD thesis. Faculdade de Ciências e Tecnologia, 2011.

[27] D. A. F. d. Almeida. "The role of electron transfer in DNA building blocks: evaluation of strand breaks and their implications". PhD thesis. Faculdade de Ciências e Tecnologia, 2013.

[28] J. Aten and J. Los. "Space charge related energy deficit in beams from charge exchange sources". In: *Journal of Physics E: Scientific Instruments* 8.5 (1975), p. 408.

[29] R. Compton, H. Carman Jr, C. Desfrancois, H. Abdoul-Carime, J. Schermann, J. Hendricks, S. Lyapustina, and K. Bowen. "On the binding of electrons to nitromethane: Dipole and valence bound anions". In:*The Journal of chemical physics* 105.9 (1996), pp. 3472–3478.

[30] L. Sanche. "Role of secondary low energy electrons in radiobiology and chemoradiation therapy of cancer". In: *Chemical Physics Letters* 474.1 (2009), pp. 1–6.

[31] I. Baccarelli, F. Gianturco, E Scifoni, A. Solovyov, and E Surdutovich. "Molecular level assessments of radiation biodamage". In: *The European Physical Journal D-Atomic, Molecular, Optical and Plasma Physics* 60.1 (2010), pp. 1–10.

[32] J. Simons. "How do low-energy (0.1-2 eV) electrons cause DNA-strand breaks?" In: *Accounts of chemical research* 39.10 (2006), pp. 772–779.

[33] J. Gu, J. Leszczynski, and H. F. Schaefer III. "Interactions of electrons with bare and hydrated biomolecules: From nucleic acid bases to DNA segments". In: *Chemical reviews* 112.11 (2012), pp. 5603–5640.

[34] C. König, J. Kopyra, I. Bald, and E. Illenberger. "Dissociative electron attachment to phosphoric acid esters: the direct mechanism for single strand breaks in DNA". In: *Physical review letters* 97.1 (2006), p. 018105.

[35] J. Kopyra. "Low energy electron attachment to the nucleotide deoxycytidine monophosphate: direct evidence for the molecular mechanisms of electron-induced DNA strand breaks". In: *Physical Chemistry Chemical Physics* 14.23 (2012), pp. 8287–8289.

[36] P. Papp, P. Shchukin, and Š. Matejčík. "Specific formation of negative ions from leucine and isoleucine molecules". In: *The Journal of chemical physics* 132.1 (2010), p. 014301.

[37] S Ptasińska, S Denifl, P Candori, S Matejcik, P Scheier, and T. Märk. "Dissociative electron attachment to gas phase alanine". In:*Chemical physics letters* 403.1 (2005), pp. 107–112.

[38] J. Kopyra. "Electron attachment to the N-substituted amino acids N-methylglycine and N-methylalanine: Effective cleavage of the N–Cα bond at sub-excitation energies". In: *Chemical Physics Letters* 533 (2012), pp. 87–91.

[39] H. Abdoul-Carime, S. Gohlke, and E. Illenberger. "Site-specific dissociation of DNA bases by slow electrons at early stages of irradiation". In: *Physical review letters* 92.16 (2004), p. 168103.

[40] P. Papp, J. Urban, Š. Matejčík, M. Stano, and O. Ingolfsson. "Dissociative electron attachment to gas phase valine: A combined experimental and theoretical study". In: *The Journal of chemical physics* 125.20 (2006), p. 204301.

[41] D. Almeida, F. F. da Silva, G. García, and P. Limão-Vieira. "Selective bond cleavage in potassium collisions with pyrimidine bases of DNA". In: *Physical review letters* 110.2 (2013), p. 023201.

[42] D. Almeida, F. F. da Silva, G. García, and P. Limão-Vieira. "Dynamic of negative ions in potassium-D-ribose collisions". In: *The Journal of chemical physics* 139.11 (2013), p. 114304.

[43] D. Almeida, F. Ferreira da Silva, S. Eden, G. Garcia, and P. Limão-Vieira. "New Fragmentation Pathways in K–THF Collisions As Studied by Electron-Transfer Experiments: Negative Ion Formation". In: *The Journal of Physical Chemistry A* 118.4 (2014), pp. 690–696.

[44] F. Ferreira da Silva, J. Rafael, T. Cunha, D. Almeida, and P. Limão-Vieira. "Electron transfer to aliphatic amino acids in neutral potassium collisions". In: *International Journal of Mass Spectrometry* 365 (2014), pp. 238–242.

[45] F. F. da Silva, C. Matias, D. Almeida, G. García, O. Ingólfsson, H. D. Flosadóttir, B. Ómarsson, S. Ptasinska, B. Puschnigg, P. Scheier, P. Limão-Vieira, and S. Denifl. "NCO–, a Key Fragment Upon Dissociative Electron Attachment and Electron Transfer to Pyrimidine Bases: Site Selectivity for a Slow Decay Process". In: *Journal of the American Society for Mass Spectrometry* 24.11 (2013), pp. 1787–1797.

[46] F. F. da Silva, D. Almeida, R. Antunes, G. Martins, Y. Nunes, S. Eden, G. Garcia, and P. Limão-Vieira. "Electron transfer processes in potassium collisions with 5-fluorouracil and 5-chlorouracil". In: *Physical Chemistry Chemical Physics* 13.48 (2011), pp. 21621–21629.

[47] Y.-F. Wang, S. X. Tian, and J. Yang. "Resonant dissociative electron attachments to cysteine and cystine". In: *Physical Chemistry Chemical Physics* 13.34 (2011), pp. 15597–15602.

[48] J. Kopyra, I. Szamrej, H. Abdoul-Carime, B. Farizon, and M. Farizon. "Decomposition of methionine by low energy electrons". In: *Physical Chemistry Chemical Physics* 14.22 (2012), pp. 8000–8004.

[49] J. Kopyra, S. Freza, H. Abdoul-Carime, M. Marchaj, and P. Skurski. "Dissociative electron attachment to gas phase thiothymine: experimental and theoretical approaches". In: *Physical Chemistry Chemical Physics* 16.11 (2014), pp. 5342–5348.

[50] J. Kopyra, H. Abdoul-Carime, F. Kossoski, and M. d. N. Varella. "Electron driven reactions in sulphur containing analogues of uracil: the case of 2-thiouracil". In: *Physical Chemistry Chemical Physics* 16.45 (2014), pp. 25054–25061.

[51] R. Lourenco and M. Camilo. "Taurine: a conditionally essential amino acid in humans? An overview in health and disease". In: *Nutricion Hospitalaria* 17.6 (2002), pp. 262–270.

[52] T. C. Birdsall. "Therapeutic applications of taurine." In: *Alternative medicine review: a journal of clinical therapeutic* 3.2 (1998), pp. 128–136.

[53] A. Brugarolas and M. Gosalvez. "Treatment of cancer by an inducer of reverse transformation". In: *The Lancet* 315.8159 (1980), pp. 68–70.

[54] M. Suo, K.-i. Mukaisho, A. Shimomura, H. Sugihara, and T. Hattori. "Thioproline prevents carcinogenesis in the remnant stomach induced by duodenal reflux". In: *Cancer letters* 237.2 (2006), pp. 256–262.

[55] V Busiello, M Di Girolamo, C Cini, and C De Marco. "Action of thiazolidine-2-carboxylic acid, a proline analog, on protein synthesizing systems". In: *Biochimica et Biophysica Acta (BBA)-Nucleic Acids and Protein Synthesis* 564.2 (1979), pp. 311–321.

[56] J. M. D. Rafael. "Decomposição de aminoácidos alifáticos por transferência de electrão em colisões átomo-molécula". MA thesis. Faculdade de Ciências e Tecnologia, 2013.

[57] W. Wiley and I. H. McLaren. "Time-of-flight mass spectrometer with improved resolution". In: *Review of Scientific Instruments* 26.12 (1955), pp. 1150–1157.

[58] I. Bald. "Low energy electron induced reactions in gas phase biomolecules". PhD thesis. Freie Universität Berlin, 2007.

[59] A. Stamatovic and G. Schulz. "Characteristics of the trochoidal electron monochromator". In: *Review of Scientific Instruments* 41.3 (1970), pp. 423–427.

[60] D. Klar, M. Ruf, and H. Hotop. "Attachment of electrons to molecules at submillielectronvolt resolution". In: *Chemical physics letters* 189.4 (1992), pp. 448–454.

[61] W. M. Haynes. *CRC handbook of chemistry and physics*. CRC press, 2013.

[62] R. Chang. "Química, 5ª edição". In: *Lisboa: MacGraw-Hill* (1994).

[63] J. Zhao, X. Cheng, and X. Yang. "Theoretical studies of C–NH 2 bond dissociation energies for some amino compounds". In: *Journal of Molecular Structure: THEOCHEM* 766.2 (2006), pp. 87–92.

[64] H. Abdoul-Carime, S. Gohlke, and E. Illenberger. "Conversion of amino-acids by electrons at subexcitation energies". In: *Physical Chemistry Chemical Physics* 6.1 (2004), pp. 161–164.

[65] A. Mauracher, S. Denifl, A. Aleem, N. Wendt, F. Zappa, P. Cicman, M. Probst, T. Märk, P. Scheier, H. Flosadóttir, O. Ingólfsson, and E. Illenberger. "Dissociative electron attachment to gas phase glycine: Exploring the decomposition pathways by mass separation of isobaric fragment anions". In:*Physical Chemistry Chemical Physics* 9.42 (2007), pp. 5680–5685.

[66] V. Cortijo, M. E. Sanz, J. C. López, and J. L. Alonso. "Conformational Study of Taurine in the Gas Phase†". In: *The Journal of Physical Chemistry A* 113.52 (2009), pp. 14681–14683.

[67] M. A. Spackman, P. Munshi, and B. Dittrich. "Dipole Moment Enhancement in Molecular Crystals from X-ray Diffraction Data". In: *Chemical Physics and Physical Chemistry* 8.14 (2007), pp. 2051–2063.

[68] R. Lobo, A. Moutinho, K Lacmann, and J Los. "Excitation of the nitro group in nitromethane by electron transfer". In: *The Journal of chemical physics* 95.1 (1991), pp. 166–175.

[69] F. Ferreira da Silva, M. Lança, D. Almeida, G. García, and P. Limão-Vieira. "Anionic fragmentation of glycine upon potassium-molecule collisions". In: *The European Physical Journal D-Atomic, Molecular, Optical and Plasma Physics* 66.3 (2012), pp. 1–7.

[70] H. Abdoul-Carime and E. Illenberger. "Fragmentation of proline induced by slow electrons". In: *Chemical physics letters* 397.4 (2004), pp. 309–313.

[71] P. Sulzer, E. Alizadeh, A. Mauracher, T. D. Märk, and P. Scheier. "Detailed dissociative electron attachment studies on the amino acid proline". In: *International Journal of Mass Spectrometry* 277.1 (2008), pp. 274–278.

[72] K. Aflatooni, B. Hitt, G. A. Gallup, and P. Burrow. "Temporary anion states of selected amino acids". In: *The Journal of Chemical Physics* 115.14 (2001), pp. 6489–6494.

[73] S. Gohlke, A. Rosa, E. Illenberger, F. Bruning, and M. A. Huels. "Formation of anion fragments from gas-phase glycine by low energy (0-15 eV) electron impact". In: *Journal of Chemical Physics* 116 (2002), pp. 10164–10169.

[74] W. Sailer, A. Pelc, M. Probst, J. Limtrakul, P. Scheier, E. Illenberger, and T. D. Märk. "Dissociative electron attachment to acetic acid (CH 3 COOH)". In: *Chemical physics letters* 378.3 (2003), pp. 250–256.

[75] T. N. Rescigno, C. S. Trevisan, and A. E. Orel. "Dynamics of low-energy electron attachment to formic acid". In: *Physical review letters* 96.21 (2006), p. 213201.

[76] M. Ahmed, A. Ganesan, F. Wang, V. Feyer, O. Plekan, and K. C. Prince. "Photoelectron spectra of some antibiotic building blocks: 2-azetidinone and thiazolidine-carboxylic acid". In: *The Journal of Physical Chemistry A* 116.33 (2012), pp. 8653–8660.